How microbial communities shape peatland carbon dynamics: New insights and implications

Etienne Richy, Pedro Cabello-Yeves, Felipe Hernandes-Coutinho, Francisco Rodriguez-Valera, Iván González-Álvarez, Laure Gandois, François Rigal, Béatrice Lauga

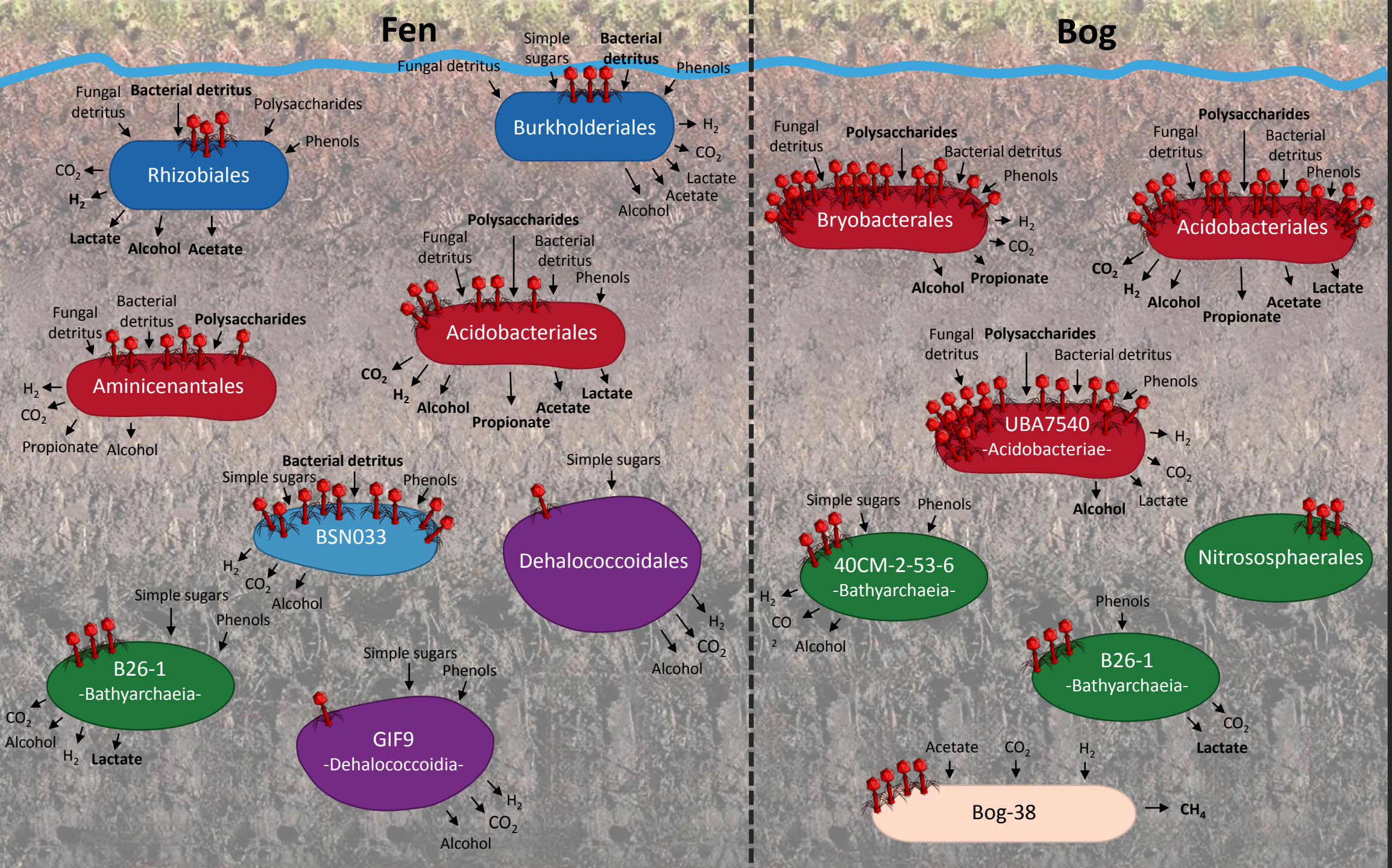
Fen
Bog
Water-table depth
fen/bog delimitation
Virus
Proteobacteria
Acidobacteriota
Desulfobacterota
Chloroflexota
Crenarchaeota
Halobacterota
Rhizobiales
Fungal detritus
Bacterial detritus
Polysaccharides
Phenols
Lactate
Alcohol
Acetate
Burkholderiales
Simple sugars
Aminicenantales
Propionate
Acidobacteriales
Propionate
BSN033
Dehalococcoidales
B26-1
-Bathyarchaeia-
GIF9
-Dehalococcoidia-
Bryobacterales
Propionate
UBA7540
-Acidobacteriae-
40CM-2-53-6
-Bathyarchaeia-
Nitrososphaerales
Bog-38

How microbial communities shape peatland carbon dynamics: new insights and implications

Etienne Richy[a,*], *Pedro J. Cabello-Yeves*[b,e,f], *Felipe Hernandes-Coutinho*[b,d], *Francisco Rodriguez-Valera*[b], *Iván González-Álvarez*[a], *Laure Gandois*[c], *François Rigal*[a] *& Béatrice Lauga*[a,*]

[a] Universite de Pau et des Pays de l'Adour, E2S UPPA, CNRS, IPREM, Pau, France

[b] Evolutionary Genomics Group, Departamento de Producción Vegetal y Microbiología, Universidad Miguel, Hernández, San Juan de Alicante, Alicante, Spain

[c] Laboratoire Écologie Fonctionnelle et Environnement, Université de Toulouse, CNRS, Toulouse, France

[d] Current affiliation: Department of Marine Biology and Oceanography, Institute of Marine Sciences (ICM), CSIC, Barcelona, Spain

[e] Cavanilles Institute of Biodiversity and Evolutionary Biology, University of Valencia, E-46980 Paterna, Valencia, Spain.

[f] Current affiliation: School of Life Sciences, University of Warwick, Coventry CV4 7AL, UK

***** Correspondence: beatrice.lauga@univ-pau.fr (B. Lauga), etiennerichy.art@gmail.com (E. Richy)

ABSTRACT

Peatlands are considered the most efficient ecosystem for long-term storage of atmospheric carbon (C). However, reasons for variations in C accumulation within peatlands remain largely unexplained. Using a comprehensive multi-level approach combining soil-atmosphere C exchanges, microbial extracellular enzyme activities, and genome-resolved cellular and viral metagenomics, we endeavored to decipher the microbial determinants and their role in C dynamics in the bog and fen of a European peatland. Overall, the bog

exhibited a higher C content and dissolved organic carbon concentration. Despite contrasting geochemical conditions, these differences were not explained by environmental parameters nor the vegetation. Metagenomic analyses revealed varying microbial community composition, the bog being less diverse and dominated by Acidobacteriota and the fen comprising five predominant phyla (Crenarcheota, Chloroflexota, Proteobacteria, Desulfobacterota and Acidobacteriota). Both bog and fen microbial communities were stable between spring and summer. Yet, similar CO_2 emissions were recorded in both bog and fen, along with similar organic matter (OM) decomposition microbial activities and potential. Ultimately, the bog harbored significantly more viruses than the fen. Most intriguingly, these viruses were predicted to target Acidobacteriota, the phyla displaying the highest OM-degrading capacity in the bog. By impairing the activity of the dominant players in OM degradation, viruses might have a significant role in C dynamics in the bog over time. In addition, we propose that low microbial diversity limited cross-feeding opportunities in the bog, further limiting C degradation. Taking together, this study deciphers the role of microbial communities driving C accumulation in peatlands and, consequently, peatland ecosystem functioning.

KEY WORDS

Peat, metagenomics, microbial diversity, microbial activities, viruses, C accumulation, ecosystem functioning

1. INTRODUCTION

Peatlands are waterlogged and predominantly anoxic environments, in which plant production is favored over microbial degradation, leading to an accumulation of carbon over time (Rydin et al., 2006). Covering only 4.632 million km^2 of the total land mass (~3%), peatlands store about one third of the total carbon (C) contained in soils (Xu et al., 2018; Yu et al., 2011), making them the most efficient ecosystem for long-term storage of atmospheric carbon. However, C accumulation rates can vary greatly between peatland types. Evidence shows that bogs tend to accumulate more C than fens (Thormann et al., 1999; Turunen et al., 2002; Watmough et al., 2022). Fens and bogs are the two major forms of northern peatlands which represent 91% of peatlands worldwide (Yu et al., 2010). Bogs receive water and nutrients from rainfall, are nutrient poor, and acidic (pH<5.5). They are dominated by *Sphagnum spp.*, which are slowly decomposed due to the presence of antimicrobial aromatic substances (e.g., polyphenols) (Bengtsson et al., 2018; Lang et al., 2009; Verhoeven and Liefveld, 1997). Fens are characterized by higher pH (pH>5.5), dominated by more easily decomposable litter from sedges, grasses, and shrubs, and fed by both precipitation and groundwater which, in turn, lead to higher nutrient concentrations (Joosten and Clarke, 2002).

Ecological gradients, trophic status, vegetation cover and hydrology are associated with the variation in C dynamics between bogs and fens, in which microbial communities play a critical role. Bogs are commonly characterized by low microbial organic matter (OM) degradation rates (Bragazza et al., 2007; Lin et al., 2012; Preston et al., 2012), carbon dioxide (CO_2) production and methane (CH_4) emissions (Abdalla et al., 2016; Danevčič et al., 2010; Webster et al., 2018) compared to fens. However, recent findings (Hoyos-Santillan et al., 2018; McGivern et al., 2021; Turetsky, 2003; Urbanová and Hájek, 2021) have challenged the view that inhibitory compounds and low nutrient concentrations – two common features of bogs – hinder OM degradation in peatlands (Abdalla et al., 2016; Dorrepaal et al., 2005; Webster et al., 2018). Consequently, our understanding of how biotic interactions influence C accumulation rates in bogs and fens remains limited. In the context of climate change, which could impair C balance in peatlands (Loisel et al., 2021), the need to decipher the mechanisms underlying C accumulation in these ecosystems – including the microbial determinants and their role in belowground C dynamics – has become critical. A comprehensive overview of C dynamics in peatlands should also take into consideration the specificity of bogs and fens (Wu and Roulet, 2014).

Given their contrasting environmental features, we first hypothesize that bogs and fens should exhibit different prokaryotic communities (Finn et al., 2020; Seward et al., 2020; St. James et al., 2021). We anticipate that the difference in C dynamics between bogs and fens should be reflected in varying capacities for OM degradation, including organic polymer hydrolysis, fermentation, methanogenesis and methanotrophy (Drake et al., 2009; Horn et al., 2003; Woodcroft et al., 2018; Ye et al., 2012). As wetland ecosystems harbor exceptional viral abundance (Williamson et al., 2017), we also hypothesize that viruses play a role in peatland C cycle. Viruses can negatively or positively influence OM degradation (Dalcin Martins et al., 2018) either by killing OM-recycling microorganisms or by manipulating the metabolisms of their hosts through the expression of auxiliary metabolic genes (AMGs) (Chen et al., 2020). To date, the role of viruses in C cycling in wetlands have mainly been examined in permafrost peatlands (Emerson et al., 2018; Trubl et al., 2021, 2018), despite representing less than half of the total peatland surface area (Hugelius et al., 2020). As permafrost soils differ in many aspects from temperate peatlands (Jansson and Taş, 2014), it is crucial to examine also their role in bogs and fens C cycling to gain a more comprehensive overview of microbial drivers of C dynamics in peatlands.

Herein, we focus on a single mountainous peatland located in the Pyrenees (Bernadouze in Ariège, France) to disentangle microbial determinants over C dynamics along a bog to fen gradient. By comparing bog and fen within the same system, our study model overcomes the inherent confounding factors (e.g., temperature, precipitation, solar radiation) that could come into play when such a comparison is undertaken at large spatial scales. To obtain a representative picture of C dynamics of the peatland, we quantified dissolved organic carbon (DOC) and organic C concentrations, C densities and estimated CO_2 and CH_4 instantaneous flux in both bog and fen sites. A total of 24 samples were collected (bog and fen at three different depths) during two seasons (spring and summer). We have adopted a comprehensive multi-level approach to investigate the full range of microbiological processes involved in C dynamics. We thus performed enzymatic assays of five key hydrolase enzymes to assess microbial OM degradation, identify the key players involved in this process by analyzing the metabolic capacity of 290 unique bacterial and archaeal metagenome-assembled genomes (MAGs). We studied environmental determinants (abiotic) on microbial diversity, composition, and activities (biotic). Lastly, the contribution of viruses to peatland functioning was assessed by ecogenomic approaches, in

which the distribution and dynamics of viruses were investigated, their hosts predicted and the putative AMGs encoded by the viruses characterized.

Collectively, our results revealed varying microbial community composition between bog and fen, the former being less diverse and dominated by Acidobacteriota and the latter comprising five predominant phyla (Crenarcheota, Chloroflexota, Proteobacteria, Desulfobacterota and Acidobacteriota). The similar CO_2 emissions and microbial OM decomposition activities and potentials recorded in bogs and fens suggested similar instantaneous ecosystem functioning with regard to carbon cycles. However, the bog harbored significantly more viruses than the fen. Most intriguingly, these viruses were predicted to target Acidobacteriota, the phyla displaying the highest OM-degrading capacity in the bog. By impairing the activity of the dominant players in OM degradation, viruses might have a significant role in C dynamics in the bog over time. In addition, we propose that low microbial diversity limits cross-feeding opportunities in the bog, further limiting C degradation. Taking together, this study deciphers the role of microbial communities driving C accumulation in peatlands and, consequently, peatland ecosystem functioning.

2. MATERIALS AND METHODS

2.1. Study Site Description and Sample Collection

Peat samples were collected at Bernadouze (42.80247 N, 1.42333 E), a mountainous peatland located at an altitude of 1,344 m in the central part of the Pyrenees (**Fig. 1A**). Bernadouze was formed from a postglacial lake, where a marsh existed for 10,000 years. This peatland covers an area of 4.7 ha, a 1.4 km^2 watershed, mainly composed of limestone (Jalut et al., 1982; Reille, 1990). The mean annual temperature recorded for the years 2015 to 2018 was 7.9 ± 0.3 ◦C and the mean annual precipitation was 1,797 ± 265 mm. Sub-zero temperatures and snowfalls are frequently recorded at Bernadouze from mid-October to mid-May (Rosset et al., 2019). The Bernadouze peatland harbors a typical peatland vegetation cover, with bogs mainly dominated by sphagnum mosses and fens by vascular plants (Joosten and Clarke, 2002).

The sampling campaigns dedicated to microbial ecogenomics were carried out during the growing season (June 12 and 13, 2018), and at the end of summer (September 4 and 5, 2018). As the fen is largely predominant

at Bernadouze (**Fig. 1A**), we over-sampled the fen compared to the bog. We collected samples from two sites in the fen and from one site in the bog. To better encompass the peatland's heterogeneity, we collected samples from both hummock and hollow at each site. For the hummocks, we used a 1 m^2 quadrat and collected three one-meter-deep cores (triplicate) using a Russian-type peat corer (5 cm × 50 cm). As the corer was 50 cm long, each core was the result of two consecutive core samplings (one replicate) to reach the depth of one meter. Samples were collected from each core at three different depths: the surface (0 to 15 cm), the middle (35 to 50 cm) and the bottom of the core (85 to 100 cm). For the hollow, triplicates were collected at ~30 cm from the edge of the hollow, maintaining a one meter distance between each core sampling. Only surface samples were collected for this microform. Each sample was subsampled in the field immediately after the core sampling and transferred directly to a liquid nitrogen container for molecular analysis. These subsamples were stored at -80°C in the lab. A second subsample was taken in the field immediately after the coring to measure the pH using Multiparameter MultiLine WTW® 3510 (Sentix 940 sensor). The remaining triplicates were pooled and mixed into a plastic bag (conserved at -20°C) for further biogeochemical analyses and enzyme activity assays. Finally, we used a piezometer to record the water table (WT) depth the following day at each sampling site. The WT depth varied between 0 and -26 cm on average, regardless of the season (Wilcoxon, p = 0.803). Considering that the average peat depth of Bernadouze has been estimated at 2 m (Jalut et al., 1982; Reille, 1990), this result indicated prevalent anoxic conditions in the peatland.

2.2. Measuring Geochemical Parameters

Peat organic carbon (C content), total nitrogen (N) and the C:N ratio of the peat samples were determined using a FLASH 2000 ThermoFisher™ elemental analyzer of water extract. Briefly, 30 g of peat were added to 150 ml of Milli-Q ultra-pure water and agitated for one night at 150 rpm and 20°C. Using a filter unit, various filtrations were carried out, including one with a Ø 80 µm nylon filter cloth, a second with a GF/A filter, a third with a GF/F filter and a final one with a 0.22µm cellulose acetate filter. The DOC concentration was also analyzed in the filtered samples, acidified to pH 2, using a TOC-5000A analyzer (Shimadzu, Japan). The nutrients (i.e. NO_2, NO_3, SO_4^{2-}, NH_4^+, PO_4^{3-}) were quantified by means of High-Performance Ion Chromatography (Dionex Ics-5000+ [anions]; Dionex DX-120 [cations]). Reference material included ION-915 and ION 96.4 (Environment and Climate Change Canada, Canada).

Soluble polyphenols were also estimated from the water extracts. Briefly, 30 g of peat were added to 150 ml of Milli-Q ultra-pure water and agitated for 1 hour. Using a 96-well microplate, 200 µl of this extract were mixed with 10 µl of 2 M of Folin-Ciocalteu reagent and 30 µl of Na_2CO_3 (100 g/L). After 30 min of incubation at 40°C, the absorbance wavelength was measured at 765 nm using a Synergy HTX Multi-Mode Reader machine. The standard curve was calculated using gallic acid at concentrations of 0, 5, 10, 20, 30, 40, 50 and 60 $mg.L^{-1}$. The phenolic content is expressed as a gallic acid equivalent, in mg/g of peat dry weight.

Total polyphenols were also extracted. A solution composed of methanol, H_2O and HCl (75/24.5/0.5) was added to fresh peat, maintaining a 1/100 ratio (w/v). Samples were agitated in the dark for 2 hours at 160 rpm and 35°C and further centrifuged at 5000 rpm for 10 min at 20 °C. Then, the peat extract was diluted with water, maintaining a 1/10 ratio (v/v), and added to 10 µl of 2 M Folin-Ciocalteu reagent mixed and incubate for 2 min. Next, 30 µl of Na_2CO_3 (100 g/L) were added and incubated for 2 hours at 20°C. The absorbance wavelength was measured at 765 nm using a Synergy HTX Multi-Mode Reader machine. The standard curve was calculated using gallic acid at concentrations of 0, 50, 100, 150, 250 and 500 $mg.L^{-1}$ diluted at 1/80. The phenolic content is expressed as a gallic acid equivalent, in mg/g of peat dry weight.

2.3. Measuring Fluxes Using Static Chambers

During snow-free periods, soil to atmosphere greenhouse gas (GHG) exchanges were measured monthly using static chambers. Collars had been installed 1 month prior to the first measurements in May 2016. For each station, measurements were first performed using a transparent acrylic chamber (30 cm diameter and 30 cm high) to measure the NEE (net ecosystem exchange). The measurement was then repeated in the dark by covering the chamber with an opaque aluminum cover to measure the ER (ecosystem respiration). Changes in CO_2 and CH_4 concentrations within the chamber headspace were monitored respectively using a CARBOCAP® GMP 343 CO2 probe (VAISALA) placed at the top of the chamber for CO_2 and a LI-COR LI-7810 analyzer connected to the chamber for CH_4.

CO_2 and CH_4 fluxes were then calculated from the linear regression of the concentrations within the chamber over time, using the following equation:

178 $$F_{co_2,CH_4} = \frac{d_{CO_2,CH_4}}{dt} * \frac{h}{1000} * \frac{Pa}{R * Ta}$$

179

180 where F is the CO_2 or CH_4 flux (µmol·m^{-2}·s^{-1}); d_{CO_2, CH_4}/dt is the variation in gas concentrations within the
181 chamber as a function of time (ppm s^{-1}); h is the total headspace height (chamber + soil collar; mm); Pa is the
182 atmospheric pressure (J m^{-3}); R is the ideal gas constant of 8.3144621 (J K^{-1} mol^{-1}); and Ta is the air temperature
183 in the chamber (K). Finally, the gross primary production (GPP) was calculated as GPP = ER - 1*NEE.

184

185 ## 2.4. Enzymatic Activity Assays

186 Microbial depolymerization activities of phenolic and lignin-type compounds were quantified through phenol
187 oxidase (laccase) and peroxidase enzymatic activities, respectively, using 2,2'-Azino-bis(3-
188 Ethylbenzthiazoline-6-Sulfonic Acid) (ABTS) as a substrate. Briefly, 50 ml of acetate buffer (0.1 M, pH = 4)
189 were mixed with 0.5 g of fresh peat. In a 96-well microplate, 200 µl of solution were mixed with 50 µl of ABTS
190 (0.1 M), incubated in the dark for 15 min at 21°C and agitated at 150 rpm. The peroxidase enzymatic activity
191 was estimated using the same protocol, adding 10 µl of H_2O_2 (0.3%) to the reaction. The reaction was stopped
192 by centrifugation at 5700 rpm for 5 min at 21°C. Fluorescence was measured at 420 nm in 150 µl of solution
193 using a Synergy HTX Multi-Mode Reader machine. Both phenol oxidase and peroxidase are expressed in
194 µmol.min^{-1}.g^{-1} of peat dry weight. Acid phosphate (phosphatase), chitinase and B-glucosidase enzymatic
195 activities were quantified following the BSI Standards Publication DD ISO TS 22939:2010.

196

197 ## 2.5. DNA Extraction, Sequencing, Assembly and Read Analysis

198 Triplicates of the subsamples were pooled and homogenized in a mortar using a pestle under liquid nitrogen.
199 The DNA extraction of the 24 subsamples was performed using the DNeasy PowerSoil kit following the
200 manufacturer's instructions (MoBio Laboratories, UK). Library preparation (PCR-free libraries) and sequencing
201 was performed using an Illumina NovaSeq 6000 platform producing 150 bp paired-end reads, at the University
202 of Maryland School of Medicine (USA). A total of 0.6 Tb of metagenomic reads data (from 18 to 47 Gb per
203 sample) were obtained. Two of the 24 metagenomes (hummock surface in bog and fen of summer sampling

campaign) were also sequenced using Pacbio Sequel II 8M SMRT Cell Run (30-hour movie). The library preparation (with size selection) and the sequencing were also performed at the University of Maryland School of Medicine (USA). For PacBio sequencing, DNA extraction was performed using the DNeasy PowerSoil Pro kit with slight optimization to avoid DNA shearing (no vortex, gentle homogenizations).

To eliminate sequencing errors from the metagenomic raw reads, we use Trimmomatic (v0.36) (Bolger et al., 2014) with the following parameters: PE, -phred33, ILLUMINACLIP:adapters.fa:2:30:10, LEADING:3, TRAILING:3, SLIDINGWINDOW:4:15, MINLEN:50. This process involved either removing reads with errors or trimming specific regions within the read sequences, such as low-quality regions or adapters. Next, the metagenomes were assembled independently using IDBA-UD (v1.1.1) (Peng et al., 2012) with the following parameters: mink, 60; maxk, 120; step, 10 -pre-correction. We obtained 14 Gbp of contiguous sequences, of which 3 Gbp (21.4%) were > 5 kb. Long reads were assembled using hybrid SPADes (v3.13.1) (Prjibelski et al., 2020), using the corresponding paired-end Illumina metagenomes with the following parameters: only assembler -k 71,81,91,101,111,121. We obtained approximately 10 million reads per sample, with an average length of 7 kb. More than 14000 sequences were > 10kb in length, with an average length of 23 kb (**Table S1**). The Pacbio data were used to assemble additional high-quality genomes.

Unassembled 16S rRNA and 18S rRNA read fragments were obtained using USEARCH (v9.2) (Edgar, 2010) with RefSeq 16S and 18S rRNA genes as databases from December 2019 respectively, and then confirmed using ssu-align (v0.1.1) (Nawrocki and Eddy, 2010). To provide a taxonomic classification (Cabello-Yeves et al., 2020), reads were mapped using BLASTn (v2.9.0) (Altschul et al., 1990) against the SILVA database v138 from December 2019 (Quast et al., 2012) using a maximum e-value of 1×10^{-5}. In total, we identified 44012 16S rRNA and 2252 18S rRNA sequences representing 1,834 ± 382 and 94 ± 95 sequences per sample respectively. Among the 18S rRNA sequences identified, 72 were fungal sequences, representing 3 ± 4 sequences per sample.

2.6. Estimating microbial abundance

qPCR was employed to estimate total prokaryote and fungal abundances. For prokaryotes, the 16S rRNA gene was amplified using the primer pairs 341F (5′-CCTACGGGAGGCAGCAG-3) and 514R (5′-

231 ATTCCGCGGCTGGCA-3′), and a standardized commercial plasmid of E. coli (pk3) 16S rRNA gene (X80731.1)
232 was used as a standard. For fungi, the 18S rRNA gene was amplified using the primer pairs nu-SSU-1196F (5'-
233 GGAAACTCACCAGGTCCAGA-3) and nu-SSU-1536R (5'-ATTGCAATGCYCTATCCCCA-3'). The primer set was
234 validated on the peatland DNA extractions. An 18S standard was built from one of those PCR products after it
235 has been purified using illustra GFX™ PCR DNA and a Gel Band Purification Kit (GE Healthcare) following the
236 manufacturer's instructions and cloned using pGEM®-T Easy vector ligation (Promega). Transformation of the
237 recombinant plasmid was performed using One Shot™ TOP10 Chemically Competent E. coli (Invitrogen)
238 according to the manufacturer's protocol. After overnight incubation in LB Agar (Conda Pronadisa)
239 supplemented with ampicillin (100 mg.ml^{-1}), X-gal (20 mg.ml^{-1}) and IPTG (200 mg.ml^{-1}), colonies possessing
240 the insert were replicated in an LB Broth medium (Conda Pronadisa) under the same ampicillin condition and
241 incubated overnight. Plasmids were extracted using the QIAprep Spin Miniprep Kit (QIAGEN) according to the
242 manufacturer's protocol and verified in agarose 1% gel. The linearization of the final plasmid product was
243 performed by enzymatic digestion with the PstI enzyme (New England Biolabs) and then quantified using the
244 Quant-iT™ PicoGreen™ dsDNA Assay Kit (Invitrogen). The plasmid insert was sequenced and analyzed using
245 the NCBI "BLAST" analysis tool and matched at 99.70% of identity (e-value: 2e- 163) with fungal sp. strain
246 2P1CQ1 (MH429421.1).

247 Each PCR reaction was set up in a 96-well plate using 10 µl Takyon™ No Rox SYBR® MasterMix dTTP Blue
248 (Eurogentec)1x, 2 µl Forward/Revers primers, 1 µl of DNA sample and 4 µl of water (20 µl of total volume).
249 qPCR was performed on a LightCycler® 480 96-Multiwell Plates instrument (Roche Diagnostics), with an initial
250 denaturation and Takyon™ activation at 95 °C for 3 min, followed by 40 cycles of denaturation at 95 °C for 3
251 min, annealing at 60 °C for 30 s and extension time at 72 °c during 20 s for the 16S primer set and 40 s for the
252 18S primer set. The samples were run in triplicates, and qPCR plates included standard curves in duplicate and
253 a negative control. Absolute copy number quantification was calculated by plotting Cycle threshold (Ct) values
254 against the standard curve of a 10-fold dilution series of the plasmid copy number concentration. Microbial
255 abundance was corrected by soil dry weight to normalize the copy number data set.

256

257 ## 2.7. Genome Binning, MAG Quality Assessment and Annotation

MAGs were obtained using MetaBAT2 (v2.12.1) (Kang et al., 2019) and manual curation. Briefly, contigs longer than 5 kb (Illumina) and 10kb (PacBio) were indexed aligned to short read sequences. Next, SAMtools (v1.10) was used to sort BAM files and each contig coverage depth was calculated using Bowtie2 (2.3.5) (Langmead and Salzberg, 2012). This information was used to apply binning by coverage (Metabat2). CheckM (v1.0.18) was used to assess completeness and contamination of each bin (Parks et al., 2015). We recovered a total of 515 genomic bins filtered by completeness (> 50%) and contamination (< 5%). To identify redundant genomes (dereplication), the average nucleotide identity (ANI) score was calculated using a cutoff ≥ 95% and only non-redundant genomes with the highest quality scores or greatest overall sizes were kept. The taxonomic assignment of the MAGs as well as the phylogenomic reconstruction were performed using GTDB-TK (v0.3.3, release R89) (Chaumeil et al., 2019), classifying 99.6% of the MAGs as new species, 43.1% as new genera and 0.1% as new families. We retained 290 unique genomes, 50 belonging to the Archaea domain and 240 to the Bacteria domain. Two MAGs assembled from Pacbio were not recovered in the Illumina binning. We recovered 75 high-quality genomes (>95% estimated completeness) across 13 of the 27 archaeal and bacterial phyla detected.

Genome abundances across samples were calculated as reads per kilobase of genome per gigabase of metagenome (RPKGs). Raw reads were mapped against MAGs using BLASTn with the following cutoffs: minimum alignment length of 50 bp, minimum identity of 95%, maximum e-value of 1×10^{-5}. We also estimated the binning efficiency of our datasets. This was determined by mapping raw reads from the metagenomes against all the dereplicated MAGs with Bowtie2. Next, the sum of the mapped reads divided by the total number of reads (i.e. a subsampling of 10 million reads) was used to obtain the average MAG representation.

To establish a robust annotation of the predicted proteins involved in the OM recycling, Carbohydrate-Active enZYmes annotation was performed using run_dbcan (v2.0.11) (Zhang et al., 2018), screened using HMMER (Eddy, 1998), DIAMOND (Buchfink et al., 2015) and Hotpep (Busk et al., 2017) against dbcan, CAZy and PPR database respectively. Only identical predictions by at least two tools were retained. MAGs metabolic pathways annotation was performed using DRAM (v1.0.0) (Shaffer et al., 2020). Genes were first annotated using Pfam, KOfam, UniProt and MEROPS database, then classified into functional categories.

2.8. Abundance-weighted Co-occurrence Network Analysis

A correlation-based network analysis was performed to evaluate abundance-weighted co-occurrences between the 290 MAGs. Co-occurrences were quantified using Spearman's rank correlations calculated between all pairs of MAGs using the RPKG values across the 24 samples, and corrected using the Benjamini-Hochberg standard false discovery rate correction. Only co-occurrences corresponding to correlations with a coefficient (rho) > 0.6 and a p-value < 0.001 were considered to build the network. Modules (i.e., clusters) were computed using the R package *igraph* (Pons and Latapy, 2005), which identifies densely connected communities via random walks. The network visualization was performed using Gephi software (Bastian et al., 2009) with the nodes representing the MAGs and the edges representing the correlations (rho >0.6 and p-value < 0.001) between MAGs.

A random forest analysis was used to test the correct assignment of MAGs to their actual module based on their environmental preferences (i.e., expressed as their individual weighting mean calculated for each environment variable using RPKG data as abundance). This analysis was performed using a set of 10,000 trees and the importance of individual variables (i.e., weighting means) in predicting the module assignment was calculated. Models were fitted using the R package *randomForest* (Liaw and Wiener, 2002).

2.9. Virus Identification, Host Prediction and putative AMG Annotation

Viral sequences were identified and annotated (AMG) by analyzing all assembled contigs through VIBRANT (v1.0.1) (Kieft et al., 2020) with default parameters. Quality (i.e., completeness and contamination) of viral sequences was estimated with CheckV (v0.6) (Nayfach et al., 2021), revealing 55 complete and high-quality genomes (completeness >= 90%). Viral sequences were clustered into 11,524 viral populations based on ANI (>= 95%) and shared genes (>= 80%). Computational viral host prediction was performed as previously described (Coutinho et al., 2020, 2019; Malki et al., 2021). The Bernadouze bacterial and archaeal MAGs were used as a set of potential host genomes against which the viral genomes were queried. Before performing this analysis, BLAST was used to identify and remove any viral sequences incorrectly binned together with the archaeal and bacterial MAGs. Three signals of virus-host association were analyzed for host prediction: shared tRNAs, homology matches, and CRISPR spacers. Viral sequences were scanned for tRNA genes through

tRNAScan-SE (v1.23) (Lowe and Chan, 2016) using the bacterial models. Viral tRNAs were then queried against the Bernadouze MAGs through BLASTn. These searches were performed with the following cutoffs: minimum alignment length of 60 bp, minimum identity of 100%, minimum query coverage of 95%, maximum of 0 mismatches and maximum e-value of 1×10^{-3}. Homology matches were performed by directly querying viral sequences against the Bernadouze MAGs through BLASTn. For these searches, the following cutoffs were used: minimum alignment length of 1,000 bp, minimum identity of 85% and maximum e-value of 1×10^{-3}. Finally, CRISPR spacers were identified among Bernadouze MAGs using CRISPRDetect (v2.2) (Biswas et al., 2016). The obtained spacers were queried against the viral sequences using BLASTn. The following cutoffs were defined for these searches: minimum identity of 100%, minimum query coverage of 100%, maximum of 0 mismatches and maximum e-value of 1. For each virus-taxon association signal detected (i.e. homology, tRNA or CRISPR), 3 points were added to the taxon if it was a CRISPR match, 2 points if it was a homology match, and 1 point if it was a shared tRNA. The taxon that displayed the highest score was defined as the host of the viral genome.

2.10. Statistical Analyses

All the following statistical analyses were implemented within the R programming environment (RStudio Team, 2020).

The map representing the location of Bernadouze was produced using the R package *sf* (Pebesma, 2018). The influence of the season on the WT depth was analyzed using a Wilcoxon signed-rank test. The difference of C content, N, C:N ratio, DOC, polyphenols (total and soluble), nutrients (SO_4^{2-}, NO_3^-, NH_4^+ and PO_4^{3-}), C accumulation (C content and C density) and soil-atmosphere C exchanges (GPP, ER, NEE) between bog and fen was tested using Wilcoxon signed-rank test. The effect of the environmental parameters on the enzyme activities was tested using an analysis of variance (ANOVA) and compared between bog and fen with a Wilcoxon signed-rank test. The link between these activities on C content was evaluated using Spearman correlations.

The difference of the 16S and 18S gene copy numbers between bog and fen was evaluated using a Wilcoxon signed-rank test. The Bray-Curtis distance was then calculated between all pairs of samples based on 16S

rRNA and viral population to study the structure of the microbial communities, and the results were visualized using non-metric multidimensional scaling ordinations (NMDS) using the function metaMDS in the package *vegan* (Oksanen, 2020). To identify the influence of the environmental variables on the community structure, a dissimilarity matrix was calculated based on Euclidean distances from the 16S rRNA gene or viral population abundance estimated in each sample. A first permutational multivariate analysis of variance tests (PerMANOVA) with 9,999 iterations (Anderson, 2001) was performed to test the influence of the experimental design namely season, sites, microforms (hummocks and hollows) and depth, including all double interactions using the function adonis2() in *vegan*. A second PerMANOVA was performed to evaluate the influence of environmental parameters (pH, distance to WT, DOC, org C, total N, total phenols, and nutrients). To avoid the presence of strong multicollinearity between the environmental variables, soluble phenols were removed from this analysis since they were strongly correlated with total phenols (Spearman's rank correlation, $r = 0.83$, $p > 0.01$) and a principal component analysis (PCA) was performed between the highly correlated nutrient variables (SO_4^{2-}, NO_3^-, NH_4^+ and PO_4^{3-}). Only the first principal component (accounting for 64%) was kept as a new composite nutrient variable. The metagenome archaeal and bacterial diversity were estimated using the 16S rRNA gene recovered in each metagenome at the species level. The exponential of Shannon ($e^{H'}$) was calculated as alpha diversity metric (Haegeman et al., 2013) using the package *vegan*. These indices were compared between metagenomes using a Wilcoxon signed-rank test.

Finally, an indicator analysis (Dufrêne and Legendre, 1997) was conducted to identify whether the genes involved in OM degradation (plant, fungal and bacterial biomass), polyphenol degradation, fermentation processes (alcohol production, butyrate, propionate, acetate and lactate), methanogenesis and methanotrophy were preferentially associated to either the bog or the fen. This association was assessed using the indicator value (Point-biserial correlation) method (Cáceres and Legendre, 2009) using the package *indicspecies*. This method combines information on the ecological specificity and fidelity of each gene calculated with its respective RPKG distribution across the 24 samples. A permutation test (N = 9,999) was used to determine whether a particular gene was significantly associated to either the bog or fen under the null hypothesis of no association.

3. RESULTS

3.1. Geochemical Context of the Bernadouze Peatland

Given the predominance of the fen at Bernadouze (**Fig. 1A**), we collected 16 samples in the fen and 8 samples in the bog. The average WT depth in the bog was -10.5 cm and -13.1 cm in the fen, indicating prevalent anoxic conditions (see methods). The pH ranged from 6.4 in the fen to 4.6 in the bog. This is consistent with a shift in vegetation cover: while forbs, sedges and other bushes dominate in the fen, S*phagnum* mosses are predominant in the bog (**Fig. 1A**). These variations are congruent with higher concentrations of soluble polyphenols (Wilcoxon, $p < 0.045$, **Table S2**), and total polyphenols ($p < 0.01$) in the bog while nutrients and N concentrations ($p = 0.569$, $p = 0.976$ respectively) were not significantly different between bog and fen. The C:N ratio did not differ between the bog and the fen ($p = 0.093$, **Table S2**), suggesting an overall similar peat decomposition.

3.2. Carbon Fluxes in Bog and Fen

We also compared the C dynamics in each peatland type by quantifying DOC, C concentration (mass of C per gram of peat) and C density (C concentration multiplied by peat bulk density) which, taken together, evidenced C accumulation. Two-sample Wilcoxon tests (**Table S3**) revealed a higher DOC concentration ($p = 0.027$) in the bog and C content ($p < 0.01$) whereas we did not observe a difference in C density ($p = 0.881$, **Fig. 1A**). Overall, the contrast in carbon properties between bog and fen suggests different biotic (decomposition) and/or abiotic (DOC hydrology and geochemistry) processes, which could affect the C dynamics in the two types of peatland. In addition, C properties varied along the peat profile with higher C density at depth in the bog (**Fig. S1**), consistent with higher C accumulations over time.

Soil-atmosphere C exchanges in the peatland were estimated by measuring field instantaneous C fluxes over six years (2016-2022). The difference between GPP (photosynthetic CO_2 uptake) and ER (autotrophic and heterotrophic CO_2 production), provides an estimation of an ecosystem's C gain and loss, summarized by the NEE. Instantaneous measurements of GPP were always higher than ER at Bernadouze, resulting in a negative NEE (**Fig. 1B**). However, neither GPP (Wilcoxon, $p = 0.675$), ER ($p = 0.401$) nor NEE ($p = 0.063$, **Table S2**)

showed significant variations between bog and fen, indicating a similar CO_2 fixation and respiration of the two types of peatland. C exchanges were governed by seasonal dynamics, with GPP and ER increasing during the summer season compared to spring, evidencing the importance of temperature and solar radiation on aboveground C dynamics. Together with peat C estimates, these results suggest that the difference in C content between bog and fen at Bernadouze is not due to varying vegetation-related C dynamics. Instead, our findings suggest that differences in belowground C dynamics between bog and fen are sustained by a difference in the magnitude of microbial decomposition.

3.3. Microbial Extracellular Enzyme Activities

We estimated heterotrophic activities related to OM degradation by quantifying the depolymerization of phenolic and lignin-like compounds (phenol oxidase and peroxidase respectively), the degradation of cellulose (ß-1,4-glucosidase), the mineralization of organic phosphorus (acid phosphatase), and the hydrolysis of chitin-derived oligomers (ß-1,4-N-acetyl-glucosaminidase). Enzyme assays revealed marginal variations between bog and fen (Wilcoxon, $p > 0.05$, **Fig. 1C**, **Table S2**), suggesting identical OM degradation. Regression analyses revealed a positive effect of nitrogen concentration on phenol oxidase ($p < 0.001$), peroxidase ($p < 0.001$) and ß-glucosidase ($p = 0.01$), a positive effect of the distance to WT on chitinase ($p = 0.047$) and phosphatase ($p = 0.003$), and a positive effect of nutrient concentration on chitinase ($p = 0.007$) (**Table S4**). In contrast, we noted a negative effect of the distance to the WT on phenol oxidase ($p < 0.001$), indicating a possible phenol degradation under anaerobic conditions. Importantly, free phenolic compound and C content concentrations failed to predict microbial enzyme activities, suggesting (i) that polyphenols do not impede OM degradation and (ii) that C is not a limiting factor for OM degradation. Collectively, these results predict complex relationships between microorganisms and C dynamics.

3.4. Structure and Functioning of Peatland Microbial Communities

We first estimated the prokaryote and fungal abundances based on 16S and 18S gene abundances using qPCR, respectively. No significant difference in prokaryotes (Two-sample Wilcoxon test, $p = 0.320$) or fungal abundances – largely underrepresented – ($p = 0.834$, **Table S2**) was evidenced between bog and fen.

Hypostatizing that a high microbial diversity promotes C degradation and CO_2 emission, we thus compared the prokaryotic diversity based on 16S (exponential of Shannon, $e^{H'}$) with C content. A strong negative correlation (Spearman's rank correlation, rho = -0.66, $p < 0.01$) suggests that higher microbial diversity promotes OM degradation at Bernadouze.

Differences in microbial composition were not significant between spring and summer (PerManova: $R^2 = 0.01$, $p = 0.968$) and between hummock and hollow ($R^2 = 0.03$, $p = 0.352$) (**Fig. 2A, Table S5**). In contrast, we detected a strong turnover between bog and fen ($R^2 = 0.29$, $p = 0.001$) and with depth ($R^2 = 0.17$, $p = 0.003$), in relation to pH ($R^2 = 0.27$, $p = 0.001$) and distance to the WT ($R^2 = 0.14$, $p = 0.001$). The bog exhibited a lower microbial diversity (Wilcoxon, $p < 0.01$) compared to the fen, highlighting environmental filtering due to the acidic conditions in the bog. Acidobacteria (27.5% of 16S sequences), Crenarchaeota (14.4%), Thaumarchaeota (11.0%) and Euryarchaeota (8.4%) were identified as the dominant phyla in the bog while (**Fig. 2B**) Crenarchaeota (15.8%), Chloroflexi (13.5%), Proteobacteria (11.8%), Deltaproteobacteria (11.6%) and Acidobacteria (10.4%) were the most abundant phyla in the fen.

To identify key microorganisms involved in OM degradation, we reconstructed 290 unique bacterial and archaeal metagenome assembled genomes (MAGs, **Fig. 2C**). MAG diversity showed a strong congruence with 16S rRNA diversity, with an average number of raw-reads mapping with MAG of 32.5% in bog and 21.2% in fen. The ecological niches occupied by these MAGs were estimated through an abundance-weighted co-occurrence network which distinguished four distinct modules (**Fig. 2C**). Using a random forest classification model, we identified the distance to the WT (0.23%), C content (0.19%) and the pH (0.17%) as the main environmental variables predicting module configuration (**Fig. 2C**). The similar contribution of pH and C content to module configuration was due to the higher amount of C at acidic pH (**Table S2**). Modules 1 (36 MAGs) and 4 (81 MAGs) were comprised of MAGs abundant at low pH (pH 5 on average, corresponding to bog conditions) and assigned to deep peat layers for module 1 (-40 cm below the WT) and to the subsurface (-10 cm below the WT) for module 4 (**Fig. 2C**). The prevalent MAGs (42.7 RPKG on average) were mainly affiliated to the Acidobacteriota and Crenarchaeota phyla. Modules 2 (116 MAGs) and 3 (55 MAGs) were composed of MAGs abundant at circumneutral pH (pH 6.4 on average, corresponding to fen conditions) and were also assigned to deep peat layers for module 2 and to the subsurface for module 3 (**Fig. 2C**). These MAGs were less abundant on average (26.7 RPKG) but more diverse, mainly belonging to the Crenarchaeota, Chloroflexota,

Acidobacteriota, Proteobacteria and Desulfobacterota (Deltaproteobacteria) phyla. Combined with the 16S rRNA based diversity, these results confirm that the structure of microbial communities in the Bernadouze peatland was driven by pH and depth.

3.5. Role of Microorganisms in OM Degradation

We examined the CAZYme genes involved in the degradation of OM compounds derived from plants, bacteria and fungi, as well as genes involved in fermentative, methanogenic and methanotrophic pathways (**Fig. 3**, **Table S6**). Overall, a large number of MAG-encoded genes involved in the first steps of OM degradation were recovered, highlighting the importance of these processes in peatland C cycling. Particularly, the high abundance of genes involved in the breakdown of cellulose and hemicellulose -which require multiple enzymes- indicated high plant degradation capability. Importantly, 38.3% of MAG encoded genes were involved in phenol degradation, suggesting that phenols can commonly be used as an energy source. In addition, we also found that some abundant groups in the fen such as Gammaproteobacteria, BSN033 (Desulfobacterota) or UBA9217 (Nitrospirota), encoded more genes involved in bacterial than plant OM recycling, which may represent a strategic energy resource under limited OM supply.

An indicator analysis testing the association between pathways and peatland types did not reveal any specific association between pathways and peatland types, indicating that most pathways were found both in fen and bog in similar abundance (**Table S7**). However, phyla contribution to each pathway (expressed here as % of RPKG) greatly varied between bog and fen. Importantly, primary functions involved in plant, fungal and bacterial biomass degradation were mostly harbored by the class of Acidobacteriae in the bog (ranging from 61% for plant degradation to 68% for bacterial degradation **Table S8**), surpassing the degradation capacity of Bacteroidia (8% for plant and 14% for fungal) and other taxa (**Fig. 3, Table S8**). In contrast, phyla contribution to each pathway was more evenly distributed in the fen (**Table S8)**. Acidobacterota appeared as a keystone taxa associated with OM degradation in the Bernadouze peatland and more particularly in the bog.

Subsequent degradation can occur by multiple fermentation processes, including lactate and acetate, but the presence of Acidobacteriae significantly increases the capacity to produce propionate and alcohol in the bog, since they encoded 77% and 60% of this fermentative capacity respectively. Ethanol is an important precursor

of hydrogenotrophic methanogenesis in the acid bog, and can provide a substrate for the methanogen Bog-38, the most abundant genome assembled at Bernadouze (cumulative abundance of Bog-38 = 338 RPKG, means of 290 MAGs = 33 RPKG, **Table S9 and Fig. S2**) and predominantly recovered in the bog. Similarly to other MAG methanogens, Bog-38 is hydrogenotrophic methanogen (**Table S10**). Interestingly, CH_4 emissions were lower in the bog than in the fen ($p < 0.01$, **Table S2**), likely related to the presence of Binataceae (Binatota) and Methylocapsa (Pseudomonadota) methanotrophs that might participate in CO_2 recycling. Overall, these results reveal a similar capacity for OM degradation in the bog and in the fen, consistent with the similar microbial degradation activity and microbial abundances recorded in the two peatland types. Taken together, these results are intriguing given the marked differences in C dynamics (C content and DOC) evidenced between the bog and fen, suggesting that additional regulating processes may drive the differences in C accumulation observed between bog and fen.

3.6. Ecological Role of Viruses

We identified 14,578 virus sequences in Bernadouze, which clustered into 11,524 viral populations. As with prokaryotic diversity, viral diversity was mainly structured according to the pH (Permanova, $R^2 = 0.29$, $p = 0.001$) and the distance to WT ($R^2 = 0.21$, $p = 0.002$), and was stable over time ($p= 0.594$, **Fig. 4A**). Importantly, viruses were 2.6 times more abundant in the bog than in the fen on average (**Fig. 4B**), and viral populations for which a host was predicted (24.3%) were consistently 3 time more in the bog than in the fen (**Fig. 4C**). Across the 24 peat samples, virus abundance was strongly correlated with host abundance at the phylum level, except for poorly represented phyla (**Fig. S3**). Nevertheless, the bog and the fen exhibited contrasting patterns in terms of viral infection dynamics. In both peatland types, the virus-to-host abundance ratio was positive for most phyla, underscoring an overall high level of infection potential at Bernadouze (mean ratio: 6.6 and 9.2 in the bog and the fen respectively). However, this ratio varied greatly between phyla, ranging from 0.72 (WOR-3) to 42.66 (Fibrobacterota) in the bog, and from 0.81 (Asgardarchaeota) to 28.38 (Halobacterota) in the fen. High potential viral infections were recorded for both rare and dominant phyla (**Fig. 4D**). However, in the case of some phyla, viral infections differed widely between the bog and the fen. Notably, Acidobacteriota – which had the highest potential for OM degradation and was among the most dominant lineages in both peatland

types – showed a higher level of infection in the bog (mean virus-to-host abundance ratio of 17.65 in the bog and 6.02 in the fen).

Putative AMGs involved in OM degradation were retrieved in 11.4% of the viral sequences annotated. The most common one, galE, which encodes UDP-glucose 4-epimerase, was recovered 33 times (**Table S11**). This gene is involved in miscellaneous pathways, as it catalyzes the interconversion of UDP-galactose and UDP-glucose as part of the catabolism of galactose. Although rarely recovered at Bernadouze, putative AMGs involved in the degradation of organic cell compounds (exo-α-sialidase), pectin (pectate lyase) and aromatic compounds (mhpC, carboxymethylenebutenolidase) were also identified, as well as family 18 (chitinase) and family 20 (hexosaminidase) glycosyl hydrolases. Viruses encoding putative AMGs involved in OM degradation were significantly more abundant in the bog than in the fen ($p < 0.001$, **Table S11**). Overall, we concluded that viruses were more likely to influence the functioning of the bog than the fen.

4. DISCUSSION

We employed a multi-level approach to explain the role of microbial communities in C dynamics in bog and fen, two peatland types recognized to exhibit different C accumulation rates. Carbon accumulation is a long-term process that can take thousands of years (Yu et al., 2011, 2010). We thus investigated contemporary C dynamics through C content, DOC concentration and C density. Contemporary flux exchanges were similar between bog and fen over 6 years of record. Considering that *Sphagnum* mosses produce less biomass than vascular plants (Hobbie and Chapin, 1998), it is unlikely that the higher C content in the bog would be related to a higher OM production. These results were supported by the heterotrophic activity involved in OM degradation, also found to be similar between bog and fen. Considering that these activities are correlated with nutrient concentrations, a nutrient limitation may contribute to the C accumulation process at the peatland scale (Dorrepaal et al., 2005; Turetsky, 2003). However, nutrients cannot be considered the source of differences in C content at Bernadouze given that their concentration was determined to be similar in the bog and in the fen. Also, contrary to the "enzyme latch theory" (Fenner and Freeman, 2011; Freeman et al., 2001), which suggests that phenolic compounds can act as a "latch" to stabilize C in the peat, we did not identify any significant relationship linking polyphenols (total and soluble) and microbial extracellular enzymatic activities.

529 Moreover, 38.3% of MAGs possessed the metabolic capacity to use phenolic compounds as an energy source,
530 which thus may represent a sustainable source of OM for microorganisms, mainly under anaerobic conditions,
531 as recently demonstrated (McGivern et al., 2021).

532 The present work confirmed that Acidobacteriota, the predominant lineage in the Bernadouze peatland,
533 exhibited a high metabolic capacity for OM degradation. They encoded the largest repertoire of CAZymes in
534 the peatland, a consistent feature observed in cultivable Acidobacteria (Eichorst et al., 2007; Pankratov and
535 Dedysh, 2010; Whang et al., 2014), as well as in genomes assembled from natural environments (Diamond et
536 al., 2019; Woodcroft et al., 2018). Acidobacteriota dominated the microbial community in the bog where
537 environmental conditions fit their ecological niches (Kalam et al., 2020). Their high metabolic capacity in OM
538 degradation contrasted therefore with the C dynamics in the bog, where higher C content and DOC
539 concentration were recorded. Interestingly, we also established that the bog contained 2.6 times more viruses
540 than the fen and that bog Acidobacteriota were probably subject to higher pressure of viral infection than
541 their fen counterparts.
542 The more substantial presence of viruses in the bog , which aligns with Emerson et al. (2018) findings, might
543 be due to higher viral adsorption to soil surfaces at acidic pH (Gerba, 1984). However, not all host taxa in the
544 Bernadouze bog exhibit higher virus/host ratio. Moreover, while a higher number of virus predicted to infect
545 Acidobacteriota were also found in Stordalen, the Acidobacteriota virus/host ratio was subsequently higher in
546 Bernadouze bog (17.65) compared the thawing permafrost (0.1 to 1) (Emerson et al., 2018). These results are in
547 line to the *Kill the Winner* model, in which viruses exert a top-down control over microbial community by
548 targeting the most abundant taxa (Thingstad, 2000). The high abundance of virus predicted to infect
549 Acidobacteriota might contribute to constrain their metabolic rate (Feiner et al., 2015; Paul, 2008) and impair
550 their efficiency in degrading OM in the bog. Moreover, although we cannot evidence a difference in the viral
551 infection dynamics across the two seasons, viral shunts, that result in host-selective viral lysis and death,
552 further exacerbates their role in bog C dynamics by altering C degradation capacity. Interestingly, the release
553 of carbon and nutrients into the milieu as a consequence of cells bursting might contribute to explain the
554 higher DOC concentration we evidenced in the Bernadouze bog, a process previously suggested in the
555 Stordalen frozen peatland (Emerson et al., 2018). Consequently, we propose that the role of bog viruses may
556 be underestimated, as they impair OM degradation by primary degraders, thereby enhancing C accumulation

over time. However, we are aware that additional factors such as slow growth (Campanharo et al., 2016; Davis et al., 2011, 2005; George et al., 2011) and slower degradation rates (Pankratov et al., 2011) in Acidobacteria might also contribute to impair OM degradation in the bog.

We have also evidenced negative associations between microbial diversity and C content at Bernadouze. Consistent with previous studies (Finn et al., 2020; Seward et al., 2020; St. James et al., 2021), the bog has been characterized as having a low microbial diversity, dominated by a few lineages belonging to Acidobacteria, whereas the fen exhibits more diverse microbial communities, mainly composed of Proteobacteria, Crenarchaeota, Acidobacteria, Deltaproteobacteria and Chloroflexi. It has been demonstrated that a high microbial diversity promotes organic matter decomposition in soils (Maron et al., 2018). Therefore, the lower bog microbial diversity could also be a factor in reduced OM decomposition. It has been recognized that high microbial diversity might improve cross-feeding (Hoek and Merks, 2017), minimizing enzyme and intermediate concentrations in a pathway, maximizing ATP production within the community, and stimulating OM degradation (Pfeiffer and Bonhoeffer, 2004; Wei et al., 2009). The acidic pH prevailing in the bog would instead result in a specialization and metabolic capacity overlap (Hester et al., 2019), preventing efficient OM degradation.

Overall, these results provide evidence that bog and fen are two distinct ecosystems that not only differ by their environmental conditions but also by the composition of their prokaryotic and viral communities. Consequently, we showed that the functioning of these ecosystems, and particularly their C dynamics, is not only driven by ecological gradients, trophic status, vegetation covers and hydrology but also by unique microbial communities that directly drive OM turnover. Hence, we highlighted that a higher C content and DOC concentration in the bog, reflecting a lower OM degradation capacity, might be the result of i) a disruption in the metabolic potential of Acidobacteriota key degraders due to their susceptibility to viral predation and ii) the high specialization and metabolic overlap within the bog microbial community. Understanding the extent to which each of these processes contributes to disrupting OM degradation in bog and fen is of paramount importance to quantify the ecological and biogeochemical outcomes of peatland functions and assess their impact on C accumulation over time in the context of climate change.

DATA AVAILABILITY

Genomic data, including raw Illumina sequencing reads of the 24 metagenomes (SAMN24979748-SAMN24979725), the 2 raw Pacbio sequencing reads (SAMN26257891, SAMN26256348), the 290 MAGs (SAMN25001521-SAMN25001810), and the 11,755 viral populations (SAMN26259414) are available under NCBI BioProject accession number PRJNA797241.

AUTHOR CONTRIBUTIONS

E.R., F.R. and B.L designed the sampling strategy with the inputs from L.G. and performed the peat sampling. L.G. performed the chemical analysis and E.R. the polyphenols concentration. B.L and I.G-A designed and performed the qPCR analysis. L.G. carried out the flux measurements and E.R. the enzyme activity assays. E.R, P.J.C.Y. and F.H.C. performed genomic sequence processing, assembly, and annotation. E.R. conceived and carried out the analysis with the inputs from F.R., L.G. and B.L.. E.R., B.L. and F.R. performed the statistical analysis. E.R. wrote the first draft of the manuscript. F.R. L.G, and B.L. contributed to concept polishing, editing and critical revision. All the authors read, implemented and approved the final manuscript.

DECLARATION OF COMPETING INTEREST

The authors declare that they have no known competing financial interests or personal relationships that could have appeared to influence the work reported in this paper.

ACKNOWLEDGMENTS

The authors thank F. Julien, V. Payre-Suc and D. Lambrigot for DOC and major elements analysis (PAPC platform, EcoLab laboratory); and Simon Gascoin, Pascal Fanise, the CESBIO laboratory and the OSR Toulouse for providing the meteorological data. We are indebted to Alice Baldy and Eva Sandoval-Quintana for their fieldwork support, Vincent E. J. Jassey for his advice regarding enzyme activity assays, and Dominique Masse for the English revision of the manuscript. This project was co-funded by the LabEx DRIIHM OHM Haut

Vicdessos/Haute Vallée des Gaves (Pyrpeat project), INTERREG V POCTEFA REPLIM (project no. EFA056/15). B.L. was supported by funds from an E2S-UPPA program (Hub-MeSMic project). E.R. was supported by a PhD grant from the CDABPP (Communauté d'Agglomération Pau Béarn Pyrénées) and IPREM, and by a postdoctoral fellowship from E2S-UPPA. I. G.A. was supported by an Académie des talents graduate fellowship from E2S-UPPA program. PJC-Y was supported by an APOSTD/2019/009 Postdoctoral fellowship from Generalitat Valenciana.

References

Abdalla, M., Hastings, A., Truu, J., Espenberg, M., Mander, Ü., Smith, P., 2016. Emissions of methane from northern peatlands: a review of management impacts and implications for future management options. Ecol. Evol. 6, 7080–7102. https://doi.org/10.1002/ece3.2469

Altschul, S.F., Gish, W., Miller, W., Myers, E.W., Lipman, D.J., 1990. Basic local alignment search tool. J. Mol. Biol. 3, 403–410.

Anderson, M.J., 2001. A new method for non-parametric multivariate analysis of variance. Austral Ecol. 26, 32–46. https://doi.org/10.1111/j.1442-9993.2001.01070.pp.x

Bastian, M., Heymann, S., Jacomy, M., 2009. Gephi : an open source software for exploring and manipulating networks 2.

Bengtsson, F., Rydin, H., Hájek, T., 2018. Biochemical determinants of litter quality in 15 species of Sphagnum. Plant Soil 425, 161–176. https://doi.org/10.1007/s11104-018-3579-8

Biswas, A., Staals, R.H.J., Morales, S.E., Fineran, P.C., Brown, C.M., 2016. CRISPRDetect: A flexible algorithm to define CRISPR arrays. BMC Genomics 17, 356. https://doi.org/10.1186/s12864-016-2627-0

Bolger, A.M., Lohse, M., Usadel, B., 2014. Trimmomatic: a flexible trimmer for Illumina sequence data. Bioinformatics 30, 2114–2120. https://doi.org/10.1093/bioinformatics/btu170

Bragazza, L., Siffi, C., Iacumin, P., Gerdol, R., 2007. Mass loss and nutrient release during litter decay in peatland: The role of microbial adaptability to litter chemistry. Soil Biol. Biochem. 39, 257–267. https://doi.org/10.1016/j.soilbio.2006.07.014

Buchfink, B., Xie, C., Huson, D.H., 2015. Fast and sensitive protein alignment using DIAMOND. Nat. Methods 12, 59–60. https://doi.org/10.1038/nmeth.3176

636 Busk, P.K., Pilgaard, B., Lezyk, M.J., Meyer, A.S., Lange, L., 2017. Homology to peptide pattern for annotation
637 of carbohydrate-active enzymes and prediction of function. BMC Bioinformatics 18, 1–9.
638 Cabello-Yeves, P.J., Zemskaya, T.I., Zakharenko, A.S., Sakirko, M.V., Ivanov, V.G., Ghai, R., Rodriguez-Valera,
639 F., 2020. Microbiome of the deep Lake Baikal, a unique oxic bathypelagic habitat. Limnol. Oceanogr.
640 65, 1471–1488. https://doi.org/10.1002/lno.11401
641 Cáceres, M.D., Legendre, P., 2009. Associations between species and groups of sites: indices and statistical
642 inference. Ecology 90, 3566–3574. https://doi.org/10.1890/08-1823.1
643 Campanharo, J.C., Kielak, A.M., Castellane, T.C.L., Kuramae, E.E., Lemos, E.G. de M., 2016. Optimized
644 medium culture for *Acidobacteria* subdivision 1 strains. FEMS Microbiol. Lett. 363, fnw245.
645 https://doi.org/10.1093/femsle/fnw245
646 Chaumeil, P.-A., Mussig, A.J., Hugenholtz, P., Parks, D.H., 2019. GTDB-Tk: a toolkit to classify genomes with
647 the Genome Taxonomy Database. Bioinformatics btz848.
648 https://doi.org/10.1093/bioinformatics/btz848
649 Chen, L.-X., Méheust, R., Crits-Christoph, A., McMahon, K.D., Nelson, T.C., Slater, G.F., Warren, L.A.,
650 Banfield, J.F., 2020. Large freshwater phages with the potential to augment aerobic methane
651 oxidation. Nat. Microbiol. 5, 1504–1515. https://doi.org/10.1038/s41564-020-0779-9
652 Coutinho, F.H., Cabello-Yeves, P.J., Gonzalez-Serrano, R., Rosselli, R., López-Pérez, M., Zemskaya, T.I.,
653 Zakharenko, A.S., Ivanov, V.G., Rodriguez-Valera, F., 2020. New viral biogeochemical roles revealed
654 through metagenomic analysis of Lake Baikal. Microbiome 8, 163. https://doi.org/10.1186/s40168-020-
655 00936-4
656 Coutinho, F.H., Rosselli, R., Rodríguez-Valera, F., 2019. Trends of microdiversity reveal depth-dependent
657 evolutionary strategies of viruses in the Mediterranean. mSystems 4, e00554-19.
658 https://doi.org/10.1128/mSystems.00554-19
659 Dalcin Martins, P., Danczak, R.E., Roux, S., Frank, J., Borton, M.A., Wolfe, R.A., Burris, M.N., Wilkins, M.J.,
660 2018. Viral and metabolic controls on high rates of microbial sulfur and carbon cycling in wetland
661 ecosystems. Microbiome 6, 138. https://doi.org/10.1186/s40168-018-0522-4
662 Danevčič, T., Mandic-Mulec, I., Stres, B., Stopar, D., Hacin, J., 2010. Emissions of CO_2, CH_4 and N_2O from
663 Southern European peatlands. Soil Biol. Biochem. 42, 1437–1446.
664 https://doi.org/10.1016/j.soilbio.2010.05.004

Davis, K.E.R., Joseph, S.J., Janssen, P.H., 2005. Effects of growth medium, inoculum size, and incubation time on culturability and isolation of soil bacteria. Appl. Environ. Microbiol. 71, 826–834. https://doi.org/10.1128/AEM.71.2.826-834.2005

Davis, K.E.R., Sangwan, P., Janssen, P.H., 2011. Acidobacteria, Rubrobacteridae and Chloroflexi are abundant among very slow-growing and mini-colony-forming soil bacteria: slow-growing and mini-colony-forming soil bacteria. Environ. Microbiol. 13, 798–805. https://doi.org/10.1111/j.1462-2920.2010.02384.x

Diamond, S., Andeer, P.F., Li, Z., Crits-Christoph, A., Burstein, D., Anantharaman, K., R. Lane, K., Thomas, B.C., Pan, C., Northen, T.R., Banfield, J.F., 2019. Mediterranean grassland soil C–N compound turnover is dependent on rainfall and depth, and is mediated by genomically divergent microorganisms. Nat. Microbiol. 4, 16.

Dorrepaal, E., Cornelissen, J.H.C., Aerts, R., Wallén, B., Van Logtestijn, R.S.P., 2005. Are growth forms consistent predictors of leaf litter quality and decomposability across peatlands along a latitudinal gradient? J. Ecol. 93, 817–828. https://doi.org/10.1111/j.1365-2745.2005.01024.x

Drake, H.L., Horn, M.A., Wüst, P.K., 2009. Intermediary ecosystem metabolism as a main driver of methanogenesis in acidic wetland soil: Drivers of methanogenesis in fen soil. Environ. Microbiol. Rep. 1, 307–318. https://doi.org/10.1111/j.1758-2229.2009.00050.x

Dufrêne, M., Legendre, P., 1997. Species assemblages and indicator species: The need for a flexible asymmetrical approach. Ecol. Monogr. 67, 22.

Eddy, S.R., 1998. Profile hidden Markov models. Bioinformatics 14, 755–763. https://doi.org/10.1093/bioinformatics/14.9.755

Edgar, R.C., 2010. Search and clustering orders of magnitude faster than BLAST. Bioinformatics 26, 2460–2461.

Eichorst, S.A., Breznak, J.A., Schmidt, T.M., 2007. Isolation and characterization of soil bacteria that define Terriglobus gen. nov., in the phylum Acidobacteria. Appl. Env. Microbiol. 73, 10.

Emerson, J.B., Roux, S., Brum, J.R., Bolduc, B., Woodcroft, B.J., Jang, H.B., Singleton, C.M., Solden, L.M., Naas, A.E., Boyd, J.A., Hodgkins, S.B., Wilson, R.M., Trubl, G., Li, C., Frolking, S., Pope, P.B., Wrighton, K.C., Crill, P.M., Chanton, J.P., Saleska, S.R., Tyson, G.W., Rich, V.I., Sullivan, M.B., 2018. Host-linked soil viral ecology along a permafrost thaw gradient. Nat. Microbiol. 3, 870–880. https://doi.org/10.1038/s41564-018-0190-y

694 Feiner, R., Argov, T., Rabinovich, L., Sigal, N., Borovok, I., Herskovits, A.A., 2015. A new perspective on
695 lysogeny: prophages as active regulatory switches of bacteria. Nat. Rev. Microbiol. 13, 641–650.
696 https://doi.org/10.1038/nrmicro3527
697 Fenner, N., Freeman, C., 2011. Drought-induced carbon loss in peatlands. Nat. Geosci. 4, 895–900.
698 https://doi.org/10.1038/ngeo1323
699 Finn, D.R., Ziv-El, M., van Haren, J., Park, J.G., del Aguila-Pasquel, J., Urquiza–Muñoz, J.D., Cadillo-Quiroz, H.,
700 2020. Methanogens and methanotrophs show nutrient-dependent community assemblage patterns
701 across tropical peatlands of the Pastaza-Marañón basin, Peruvian Amazonia. Front. Microbiol. 11, 746.
702 https://doi.org/10.3389/fmicb.2020.00746
703 Freeman, C., Ostle, N., Kang, H., 2001. An enzymic "latch" on a global carbon store. Nature 409, 149–149.
704 https://doi.org/10.1038/35051650
705 George, I.F., Hartmann, M., Liles, M.R., Agathos, S.N., 2011. Recovery of as-yet-uncultured soil Acidobacteria
706 on dilute solid media. Appl. Environ. Microbiol. 77, 8184–8188. https://doi.org/10.1128/AEM.05956-11
707 Gerba, C.P., 1984. Applied and theoretical aspects of virus adsorption to surfaces, in: Adv. Appl. Microbiol.
708 Elsevier, pp. 133–168. https://doi.org/10.1016/S0065-2164(08)70054-6
709 Haegeman, B., Hamelin, J., Moriarty, J., Neal, P., Dushoff, J., Weitz, J.S., 2013. Robust estimation of microbial
710 diversity in theory and in practice. ISME J. 7, 1092–1101. https://doi.org/10.1038/ismej.2013.10
711 Hester, E.R., Jetten, M.S.M., Welte, C.U., Lücker, S., 2019. Metabolic overlap in environmentally diverse
712 microbial communities. Front. Genet. 10, 989. https://doi.org/10.3389/fgene.2019.00989
713 Hobbie, S.E., Chapin, F.S., 1998. The response of tundra plant biomass, aboveground production, nitrogen,
714 and CO2 Flux to experimental warming. Ecology 79, 1526. https://doi.org/10.2307/176774
715 Hoek, M.J.A. van, Merks, R.M.H., 2017. Emergence of microbial diversity due to cross-feeding interactions in a
716 spatial model of gut microbial metabolism. BMC Syst. Biol. 11, 56. https://doi.org/10.1186/s12918-017-
717 0430-4
718 Horn, M.A., Matthies, C., Küsel, K., Schramm, A., Drake, H.L., 2003. Hydrogenotrophic Methanogenesis by
719 Moderately Acid-Tolerant Methanogens of a Methane-Emitting Acidic Peat. Appl. Environ. Microbiol.
720 69, 74–83. https://doi.org/10.1128/AEM.69.1.74-83.2003
721 Hoyos-Santillan, J., Lomax, B.H., Turner, B.L., Sjögersten, S., 2018. Nutrient limitation or home field
722 advantage: Does microbial community adaptation overcome nutrient limitation of litter decomposition

723 in a tropical peatland? J. Ecol. 106, 1558–1569. https://doi.org/10.1111/1365-2745.12923
724 Hugelius, G., Loisel, J., Chadburn, S., Jackson, R.B., Jones, M., MacDonald, G., Marushchak, M., Olefeldt, D.,
725 Packalen, M., Siewert, M.B., Treat, C., Turetsky, M., Voigt, C., Yu, Z., 2020. Large stocks of peatland
726 carbon and nitrogen are vulnerable to permafrost thaw. Proc. Natl. Acad. Sci. 117, 20438–20446.
727 https://doi.org/10.1073/pnas.1916387117
728 Jalut, G., Delibrias, G., Dagnac', J., Mardones, M., 1982. A palaeoecological approach to the last 21 000 years in
729 the Pyrenees: The peat bog of Freychinede (alt. 1350 m, Ariege, South France) 33.
730 Jansson, J.K., Taş, N., 2014. The microbial ecology of permafrost. Nat. Rev. Microbiol. 12, 414–425.
731 https://doi.org/10.1038/nrmicro3262
732 Joosten, H., Clarke, D., 2002. Wise use of mires and peatlands: background and principles including a
733 framework for decision-making. International Peat Society ; International Mire Conservation Group,
734 Jyväskylä] : [Greifswald.
735 Kalam, S., Basu, A., Ahmad, I., Sayyed, R.Z., El-Enshasy, H.A., Dailin, D.J., Suriani, N.L., 2020. Recent
736 understanding of soil Acidobacteria and their ecological significance: a critical review. Front. Microbiol.
737 11, 580024. https://doi.org/10.3389/fmicb.2020.580024
738 Kang, D.D., Li, F., Kirton, E., Thomas, A., Egan, R., An, H., Wang, Z., 2019. MetaBAT 2: an adaptive binning
739 algorithm for robust and efficient genome reconstruction from metagenome assemblies. PeerJ 7,
740 e7359. https://doi.org/10.7717/peerj.7359
741 Kieft, K., Zhou, Z., Anantharaman, K., 2020. VIBRANT: automated recovery, annotation and curation of
742 microbial viruses, and evaluation of viral community function from genomic sequences. Microbiome 8,
743 90. https://doi.org/10.1186/s40168-020-00867-0
744 Lang, S.I., Cornelissen, J.H.C., Klahn, T., van Logtestijn, R.S.P., Broekman, R., Schweikert, W., Aerts, R., 2009.
745 An experimental comparison of chemical traits and litter decomposition rates in a diverse range of
746 subarctic bryophyte, lichen and vascular plant species. J. Ecol. 97, 886–900.
747 https://doi.org/10.1111/j.1365-2745.2009.01538.x
748 Langmead, B., Salzberg, S.L., 2012. Fast gapped-read alignment with Bowtie 2. Nat. Methods 9, 357–359.
749 https://doi.org/10.1038/nmeth.1923
750 Liaw, A., Wiener, M., 2002. Classification and regression by randomForest. R News 2, 5.
751 Lin, X., Green, S., Tfaily, M.M., Prakash, O., Konstantinidis, K.T., Corbett, J.E., Chanton, J.P., Cooper, W.T.,

752 Kostka, J.E., 2012. Microbial Community Structure and Activity Linked to Contrasting Biogeochemical
753 Gradients in Bog and Fen Environments of the Glacial Lake Agassiz Peatland. Appl. Environ. Microbiol.
754 78, 7023–7031. https://doi.org/10.1128/AEM.01750-12
755 Loisel, J., Gallego-Sala, A.V., Amesbury, M.J., Magnan, G., Anshari, G., Beilman, D.W., Benavides, J.C.,
756 Blewett, J., Camill, P., Charman, D.J., Chawchai, S., Hedgpeth, A., Kleinen, T., Korhola, A., Large, D.,
757 Mansilla, C.A., Müller, J., van Bellen, S., West, J.B., Yu, Z., Bubier, J.L., Garneau, M., Moore, T., Sannel,
758 A.B.K., Page, S., Väliranta, M., Bechtold, M., Brovkin, V., Cole, L.E.S., Chanton, J.P., Christensen, T.R.,
759 Davies, M.A., De Vleeschouwer, F., Finkelstein, S.A., Frolking, S., Gałka, M., Gandois, L., Girkin, N.,
760 Harris, L.I., Heinemeyer, A., Hoyt, A.M., Jones, M.C., Joos, F., Juutinen, S., Kaiser, K., Lacourse, T.,
761 Lamentowicz, M., Larmola, T., Leifeld, J., Lohila, A., Milner, A.M., Minkkinen, K., Moss, P., Naafs,
762 B.D.A., Nichols, J., O'Donnell, J., Payne, R., Philben, M., Piilo, S., Quillet, A., Ratnayake, A.S., Roland,
763 T.P., Sjögersten, S., Sonnentag, O., Swindles, G.T., Swinnen, W., Talbot, J., Treat, C., Valach, A.C., Wu,
764 J., 2021. Expert assessment of future vulnerability of the global peatland carbon sink. Nat. Clim. Change
765 11, 70–77. https://doi.org/10.1038/s41558-020-00944-0
766 Lowe, T.M., Chan, P.P., 2016. tRNAscan-SE On-line: integrating search and context for analysis of transfer
767 RNA genes. Nucleic Acids Res. 44, W54–W57. https://doi.org/10.1093/nar/gkw413
768 Malki, K., Sawaya, N.A., Tisza, M.J., Coutinho, F.H., Rosario, K., Székely, A.J., Breitbart, M., 2021. Spatial and
769 temporal dynamics of prokaryotic and viral community assemblages in a lotic system (Manatee
770 Springs, Florida). Appl. Environ. Microbiol. 87, e00646-21. https://doi.org/10.1128/AEM.00646-21
771 Maron, P.-A., Sarr, A., Kaisermann, A., Lévêque, J., Mathieu, O., Guigue, J., Karimi, B., Bernard, L., Dequiedt,
772 S., Terrat, S., Chabbi, A., Ranjard, L., 2018. High Microbial Diversity Promotes Soil Ecosystem
773 Functioning. Appl. Environ. Microbiol. 84, e02738-17. https://doi.org/10.1128/AEM.02738-17
774 McGivern, B.B., Tfaily, M.M., Borton, M.A., Kosina, S.M., Daly, R.A., Nicora, C.D., Purvine, S.O., Wong, A.R.,
775 Lipton, M.S., Hoyt, D.W., Northen, T.R., Hagerman, A.E., Wrighton, K.C., 2021. Decrypting bacterial
776 polyphenol metabolism in an anoxic wetland soil. Nat. Commun. 12, 2466.
777 https://doi.org/10.1038/s41467-021-22765-1
778 Nawrocki, E.P., Eddy, S.R., 2010. ssu-align: a tool for structural alignment of SSU rRNA sequences.
779 Nayfach, S., Camargo, A.P., Schulz, F., Eloe-Fadrosh, E., Roux, S., Kyrpides, N.C., 2021. CheckV assesses the
780 quality and completeness of metagenome-assembled viral genomes. Nat. Biotechnol. 39, 578–585.

https://doi.org/10.1038/s41587-020-00774-7

Oksanen, J., 2020. Vegan: ecological diversity 12.

Pankratov, T.A., Dedysh, S.N., 2010. *Granulicella paludicola* gen. nov., sp. nov., *Granulicella pectinivorans* sp. nov., *Granulicella aggregans* sp. nov. and *Granulicella rosea* sp. nov., acidophilic, polymer-degrading acidobacteria from Sphagnum peat bogs. Int. J. Syst. Evol. Microbiol. 60, 2951–2959. https://doi.org/10.1099/ijs.0.021824-0

Pankratov, T.A., Ivanova, A.O., Dedysh, S.N., Liesack, W., 2011. Bacterial populations and environmental factors controlling cellulose degradation in an acidic Sphagnum peat: cellulose degradation in acidic peat. Environ. Microbiol. 13, 1800–1814. https://doi.org/10.1111/j.1462-2920.2011.02491.x

Parks, D.H., Imelfort, M., Skennerton, C.T., Hugenholtz, P., Tyson, G.W., 2015. CheckM: assessing the quality of microbial genomes recovered from isolates, single cells, and metagenomes. Genome Res. 25, 1043–1055. https://doi.org/10.1101/gr.186072.114

Paul, J.H., 2008. Prophages in marine bacteria: dangerous molecular time bombs or the key to survival in the seas? ISME J. 2, 579–589. https://doi.org/10.1038/ismej.2008.35

Pebesma, E., 2018. Simple Features for R: Standardized Support for Spatial Vector Data. R J. 10, 439. https://doi.org/10.32614/RJ-2018-009

Peng, Y., Leung, H.C.M., Yiu, S.M., Chin, F.Y.L., 2012. IDBA-UD: a de novo assembler for single-cell and metagenomic sequencing data with highly uneven depth. Bioinformatics 28, 1420–1428. https://doi.org/10.1093/bioinformatics/bts174

Pfeiffer, T., Bonhoeffer, S., 2004. Evolution of cross-feeding in microbial populations. Am. Nat. 163, E126–E135. https://doi.org/10.1086/383593

Pons, P., Latapy, M., 2005. Computing communities in large networks using random walks (long version). arXiv:physics/0512106.

Preston, M.D., Smemo, K.A., McLaughlin, J.W., Basiliko, N., 2012. Peatland Microbial Communities and Decomposition Processes in the James Bay Lowlands, Canada. Front. Microbiol. 3, 1–15. https://doi.org/10.3389/fmicb.2012.00070

Prjibelski, A., Antipov, D., Meleshko, D., Lapidus, A., Korobeynikov, A., 2020. Using SPAdes De Novo Assembler. Curr. Protoc. Bioinforma. 70. https://doi.org/10.1002/cpbi.102

Quast, C., Pruesse, E., Yilmaz, P., Gerken, J., Schweer, T., Yarza, P., Peplies, J., Glöckner, F.O., 2012. The

SILVA ribosomal RNA gene database project: improved data processing and web-based tools. Nucleic Acids Res. 41, D590–D596. https://doi.org/10.1093/nar/gks1219

Reille, M., 1990. Recherches pollenanalytiques dans l'extrémité orientale des Pyrénées : données nouvelles, de la fin du Glaciaire à l'Actuel. Ecol. Mediterr. 16, 317–357. https://doi.org/10.3406/ecmed.1990.1673

Rosset, T., Gandois, L., Le Roux, G., Teisserenc, R., Durantez Jimenez, P., Camboulive, T., Binet, S., 2019. Peatland contribution to stream organic carbon exports from a montane watershed. J. Geophys. Res. Biogeosciences 124, 3448–3464. https://doi.org/10.1029/2019JG005142

RStudio Team, 2020. RStudio: Integrated Development Environment for R. RStudio, PBC, Boston, MA URL http://www.rstudio.com/.

Rydin, H., Jeglum, J.K., Hooijer, A., 2006. The biology of peatlands, The biology of habitats. Oxford University Press, Oxford ; New York.

Seward, J., Carson, M.A., Lamit, L.J., Basiliko, N., Yavitt, J.B., Lilleskov, E., Schadt, C.W., Smith, D.S., Mclaughlin, J., Mykytczuk, N., Willims-Johnson, S., Roulet, N., Moore, T., Harris, L., Bräuer, S., 2020. Peatland microbial community composition is driven by a natural climate gradient. Microb. Ecol. 80, 593–602. https://doi.org/10.1007/s00248-020-01510-z

Shaffer, M., Borton, M.A., McGivern, B.B., Zayed, A.A., La Rosa, S.L., Solden, L.M., Liu, P., Narrowe, A.B., Rodríguez-Ramos, J., Bolduc, B., Gazitúa, M.C., Daly, R.A., Smith, G.J., Vik, D.R., Pope, P.B., Sullivan, M.B., Roux, S., Wrighton, K.C., 2020. DRAM for distilling microbial metabolism to automate the curation of microbiome function. Nucleic Acids Res. 48, 8883–8900. https://doi.org/10.1093/nar/gkaa621

St. James, A.R., Lin, J., Richardson, R.E., 2021. Relationship between peat type and microbial ecology in Sphagnum-containing peatlands of the Adirondack mountains, NY, USA. Microb. Ecol. https://doi.org/10.1007/s00248-020-01651-1

Thingstad, T.F., 2000. Elements of a theory for the mechanisms controlling abundance, diversity, and biogeochemical role of lytic bacterial viruses in aquatic systems. Limnol. Oceanogr. 45, 1320–1328. https://doi.org/10.4319/lo.2000.45.6.1320

Thormann, M.N., Szumigalski, A.R., Bayley, S.E., 1999. Aboveground peat and carbon accumulation potentials along a bog-fen-marsh wetland gradient in southern boreal Alberta, Canada. Wetlands 19, 305–317. https://doi.org/10.1007/BF03161761

Trubl, G., Jang, H. bin, Roux, S., Emerson, J.B., Brum, J.R., Bolduc, B., Woodcroft, B.J., Jang, H.B., Singleton, C.M., Solden, L.M., Naas, A.E., Boyd, J.A., Hodgkins, S.B., Wilson, R.M., Li, C., Frolking, S., Pope, P.B., Wrighton, K.C., Crill, P.M., Chanton, J.P., Saleska, S.R., Tyson, G.W., Rich, V.I., Sullivan, M.B., 2018. Soil Viruses Are Underexplored Players in Ecosystem Carbon Processing. Nat. Microbiol. 3, 870–880. https://doi.org/10.1038/s41564-018-0190-y

Trubl, G., Kimbrel, J.A., Liquet-Gonzalez, J., Nuccio, E.E., Weber, P.K., Pett-Ridge, J., Jansson, J.K., Waldrop, M.P., Blazewicz, S.J., 2021. Active virus-host interactions at sub-freezing temperatures in Arctic peat soil. Microbiome 9, 208. https://doi.org/10.1186/s40168-021-01154-2

Turetsky, M.R., 2003. The Role of Bryophytes in Carbon and Nitrogen Cycling. The Bryologist 106, 395–409. https://doi.org/10.1639/05

Turunen, J., Tomppo, E., Tolonen, K., Reinikainen, A., 2002. Estimating carbon accumulation rates of undrained mires in Finland–application to boreal and subarctic regions. The Holocene 12, 69–80. https://doi.org/10.1191/0959683602hl522rp

Urbanová, Z., Hájek, T., 2021. Revisiting the concept of 'enzymic latch' on carbon in peatlands. Sci. Total Environ. 779, 146384. https://doi.org/10.1016/j.scitotenv.2021.146384

Verhoeven, J.T.A., Liefveld, W.M., 1997. The ecological significance of organochemical compounds in *Sphagnum*. Acta Bot. Neerlandica 46, 117–130. https://doi.org/10.1111/plb.1997.46.2.117

Watmough, S., Gilbert-Parkes, S., Basiliko, N., Lamit, L.J., Lilleskov, E.A., Andersen, R., del Aguila-Pasquel, J., Artz, R.E., Benscoter, B.W., Borken, W., Bragazza, L., Brandt, S.M., Bräuer, S.L., Carson, M.A., Chen, X., Chimner, R.A., Clarkson, B.R., Cobb, A.R., Enriquez, A.S., Farmer, J., Grover, S.P., Harvey, C.F., Harris, L.I., Hazard, C., Hoyt, A.M., Hribljan, J., Jauhiainen, J., Juutinen, S., Kane, E.S., Knorr, K.-H., Kolka, R., Könönen, M., Laine, A.M., Larmola, T., Levasseur, P.A., McCalley, C.K., McLaughlin, J., Moore, T.R., Mykytczuk, N., Normand, A.E., Rich, V., Robinson, B., Rupp, D.L., Rutherford, J., Schadt, C.W., Smith, D.S., Spiers, G., Tedersoo, L., Thu, P.Q., Trettin, C.C., Tuittila, E.-S., Turetsky, M., Urbanová, Z., Varner, R.K., Waldrop, M.P., Wang, M., Wang, Z., Warren, M., Wiedermann, M.M., Williams, S.T., Yavitt, J.B., Yu, Z.-G., Zahn, G., 2022. Variation in carbon and nitrogen concentrations among peatland categories at the global scale. PLOS ONE 17, e0275149. https://doi.org/10.1371/journal.pone.0275149

Webster, K.L., Bhatti, J.S., Thompson, D.K., Nelson, S.A., Shaw, C.H., Bona, K.A., Hayne, S.L., Kurz, W.A., 2018. Spatially-integrated estimates of net ecosystem exchange and methane fluxes from Canadian

peatlands. Carbon Balance Manag. 13, 16. https://doi.org/10.1186/s13021-018-0105-5

Wei, H., Xu, Q., Taylor, L.E., Baker, J.O., Tucker, M.P., Ding, S.-Y., 2009. Natural paradigms of plant cell wall degradation. Curr. Opin. Biotechnol. 20, 330–338. https://doi.org/10.1016/j.copbio.2009.05.008

Whang, K.-S., Lee, J.-C., Lee, H.-R., Han, S.-I., Chung, S.-H., 2014. Terriglobus tenax sp. nov., an exopolysaccharide-producing acidobacterium isolated from rhizosphere soil of a medicinal plant. Int. J. Syst. Evol. Microbiol. 64, 431–437. https://doi.org/10.1099/ijs.0.053769-0

Williamson, K.E., Fuhrmann, J.J., Wommack, K.E., Radosevich, M., 2017. Viruses in soil ecosystems: an unknown quantity within an unexplored territory. Annu. Rev. Virol. 4, 201–219. https://doi.org/10.1146/annurev-virology-101416-041639

Woodcroft, B.J., Singleton, C.M., Boyd, J.A., Evans, P.N., Emerson, J.B., Zayed, A.A.F., Hoelzle, R.D., Lamberton, T.O., McCalley, C.K., Hodgkins, S.B., Wilson, R.M., Purvine, S.O., Nicora, C.D., Li, C., Frolking, S., Chanton, J.P., Crill, P.M., Saleska, S.R., Rich, V.I., Tyson, G.W., 2018. Genome-centric view of carbon processing in thawing permafrost. Nature 560, 49–54. https://doi.org/10.1038/s41586-018-0338-1

Wu, J., Roulet, N.T., 2014. Climate change reduces the capacity of northern peatlands to absorb the atmospheric carbon dioxide: The different responses of bogs and fens: PEATLANDS SWITCH TO C SOURCES BY 2100. Glob. Biogeochem. Cycles 28, 1005–1024. https://doi.org/10.1002/2014GB004845

Xu, J., Morris, P.J., Liu, J., Holden, J., 2018. PEATMAP: Refining estimates of global peatland distribution based on a meta-analysis. CATENA 160, 134–140. https://doi.org/10.1016/j.catena.2017.09.010

Ye, R., Jin, Q., Bohannan, B., Keller, J.K., McAllister, S.A., Bridgham, S.D., 2012. pH controls over anaerobic carbon mineralization, the efficiency of methane production, and methanogenic pathways in peatlands across an ombrotrophic–minerotrophic gradient. Soil Biol. Biochem. 54, 36–47. https://doi.org/10.1016/j.soilbio.2012.05.015

Yu, Z., Beilman, D.W., Frolking, S., MacDonald, G.M., Roulet, N.T., Camill, P., Charman, D.J., 2011. Peatlands and Their Role in the Global Carbon Cycle. Eos Trans. Am. Geophys. Union 92, 97–98. https://doi.org/10.1029/2011EO120001

Yu, Z., Loisel, J., Brosseau, D.P., Beilman, D.W., Hunt, S.J., 2010. Global peatland dynamics since the Last Glacial Maximum. Geophys. Res. Lett. 37, L13402. https://doi.org/10.1029/2010GL043584

Zhang, H., Yohe, T., Huang, L., Entwistle, S., Wu, P., Yang, Z., Busk, P.K., Xu, Y., Yin, Y., 2018. dbCAN2: a

meta server for automated carbohydrate-active enzyme annotation. Nucleic Acids Res. 46, W95–W101.

Figure legends

Figure 1. Location of the Bernadouze peatland and carbon dynamics (peat organic carbon, dissolved organic carbon, atmospheric carbon fluxes and microbial enzymatic activities related to OM degradation).

A. *1) Location of the Bernadouze peatland and sampling sites. The dots represent the locations of peat samplings and the stars the location of static chamber flux measurements. Purple and yellow color code indicates the bog and fen sites respectively. 2) Representative vegetation covers of the bog and the fen. 3) Box plots of peat organic carbon and dissolved organic carbon concentration, with n=8 for bog and n=16 for fen. Stars indicate the level of significance (** if p-value < 0.01 and *** if p-value < 0.001).*

B. *Atmospheric carbon fluxes over six-year period. Gross Primary Production (GPP), Ecosystem Respiration (ER) and Net Ecosystem Exchange (NEE), measured in the bog (30 measures across 6 years) and the fen (57 measures across 6 years) using a static chamber flux.*

C. *Comparison of enzymatic activities involved in the degradation of organic matter between bog (n=8) and fen (n=16).*

Figure 2. Environmental drivers of the microbial communities, prokaryotic diversity based on 16S rRNA gene and characterization of the Bernadouze metagenome-assembled genomes (290 dereplicated MAGs).

A. *Non-metric multidimensional scaling (NMDS) plot of 16S rRNA gene data based on Bray-Curtis distance (stress: 0.10). Below the NMDS, analyses of variance testing the effect of experimental design (Exp. Design): campaign, peatland type, microform, depth, and all possible two-way interactions, and environmental variables (Env. Param.): pH, distance to WT, DOC, C content, N, polyphenols, nutrients, on microbial community structure (16S rRNA based data) using PerMANOVA. Black dots indicate significant correlations (if p-value < 0.05).*

B. *Relative abundance of prokaryotic phyla in the bog and the fen, estimated by unassembled 16S rRNA gene reads.*

C. *Abundance-weighted co-occurrence network based on Spearman correlations calculated from the recruitment values of the 290 unique MAGs with > 50% of completeness and < 5% of contamination (top left). Only significant edges are shown (coefficient > 0.6, p-value < 0.001). The size of the nodes is proportional to the cumulative abundance of MAGs in the 24 metagenomes. The importance of environmental variables predicting module configuration, estimated by a random forest classification model, is shown in the bottom left. Spatial location of MAGs was estimated using individual weighted means calculated for each environmental variable (pH and distance to WT) using RPKG data as abundance (right).*

Figure 3. Predicted metabolic capacities of the Bernadouze MAGs.

Heatmap showing the abundance (log (abundance +1)) of MAGs-encoded CAZyme involved in plant biomass degradation (cellulose: GH1, GH3, GH116, GH5, GH6, GH9, GH12, GH45, GH8, AA9, AA10, GH7, GH48, hemicellulose: GH36, GH51, GH54, GH62, GH95, CE1, CE2, CE3, CE4, CE5, CE6, CE7, CE12, CE15, CE16, GH2, GH52, GH120, GH39, GH43, GH26, GH10, GH11, GH30, GH131, GH67, GH115, GH74, GH16, GH44, AA6), fungal biomass degradation (chitin: GH18, GH19, AA11, GH20 and glucans: GH17, GH64, GH81, GH128, GH55), bacterial biomass degradation (peptidoglycan: GH22, GH24, GH25, GH108, GH23, GH73, GH102, GH103, GH104) and polyphenol compounds degradation (K05909, AA1, AA2, K00422) in yellow to purple. The abundances of fermentative (alcohol: K00001, K00121, K04072, K13951, K13952, K13953, K13954, K13980, K18857, butyrate: K00634, K00929, K01896, propionate: K19697, K01026, acetate: K00625, K00925, K01905, K01067, lactate: K00016, K00101, K03778, K03777), methanogenic (K00399, K00401, K00402) and methanotrophic (K10944, K10945, K10946) pathways recovered in MAGs are in light blue to red. The metabolic capacities of MAGs in bog are shown in the left panels (purple frame) and in the right panels (yellow frame) for the fen. These capacities are summed at class-level and log transformed +1.

Figure 4. Environmental drivers and distribution of the viral populations at Bernadouze, predicted prokaryotic host and host-virus relationships in bog and fen

A. *NMDS plot of the viral populations using Bray-Curtis distance (stress: 0.08). Below the NMDS, analyses of variance testing the effect of experimental design (Exp. Design): campaign, peatland type, microform, depth and all possible two-way interactions, and environmental variables (Env. Param.): pH, distance to WT, DOC, C content, N, polyphenols, nutrients, on viral composition using PerMANOVA. Black dots indicate significant correlation (if p-value < 0.05).*

B. *Average viral population abundance in bog and fen samples (expressed in RPKG).*

C. *Box plot representing the average abundance of the virus for which a putative host was identified (expressed in RPKG).*

D. *Virus/host abundance ratios by host lineage. Abundances were calculated from read mapping to viral population and host genomes (both expressed in RPKG), respectively, in bog (top left panel) and in fen (bottom left panel). The dots indicate the mean ratio across samples (in bog n = 8, in fen n = 16), and the error bars indicate one standard deviation. The red line indicates the virus/host abundance ratio for the Acidobacteria phylum. The means host abundance in bog and fen are reported on the right panels.*

Figure S1. Carbon variations in bog and fens according to peat depth

Heatmap showing the variations of carbon density (A), dissolved organic carbon (B) and peat organic carbon (C) in bog (n=8) and fen (n=16).

Figure S2. Maximum likelihood phylogenomic tree of the MAGs recovered from the Bernadouze peatland and position of the Bernadouze methanogen lineages within the archaeal phylogenetic tree

A. *Maximum likelihood phylogenomic tree computed using GTDB-tk software, classifying each MAG according to its location in the reference tree, its relative evolutionary divergence and/or average nucleotide identity (ANI) with respect to the reference genomes. The tree was estimated based on the concatenated phylogeny of 120 bacterial single-copy marker genes or 122 archaeal single-copy marker genes. It includes 240 unique bacterial genomes and 50 unique archaeal genomes (> 50% of completeness and < 5% of contamination). Among them, Acidobacteriota (80 MAGs), Chloroflexota (44), Crenarchaeota (38), Proteobacteria (29), Bacteroidota (16) and Desulfobacterota (14) are the most*

represented phyla in the assemblage. In addition, 25 genomes belonging to phyla with a relative abundance of less than 1% according to 16S rRNA gene data were assembled, among which Aenigmarchaeota and Micrarchaeota (DPANN), Asgardarchaeota, Armatimonadota, Gemmatimonadota or Krumholzibacteriota.

B. *Phylogenetic tree of archaea calculated using GTDB-tk software. Reference taxa were also plotted to identify the position of Bernadouze's methanogen lineages. To highlight the position of Bog-38 (in red), the branches are collapsed either at the phylum-level (in blue) or the class-level (in green). Four MAGs exhibiting capacity for hydrogenotrophic methanogenesis were recovered, two belonging to the Bog-38 class and two to Methanomicrobia. The present tree revealed that Bog-38 is a sister taxon of the clade Methanomicrobia/Halobacteria. All these taxa share a common ancestor with the clade Methanosarcina/Methanocellia.*

Figure S3. Host virus relationships in bog and fen

Positive relationships between virus abundance and host abundance at phylum level in the bog (n=8) and in the fen (n=16). Virus and host abundance were log-10 transformed. The dotted black line represents the 1:1 ratio, and the solid black line is the result of the linear regression. The bog samples are plotted in purple and the fen samples in yellow.

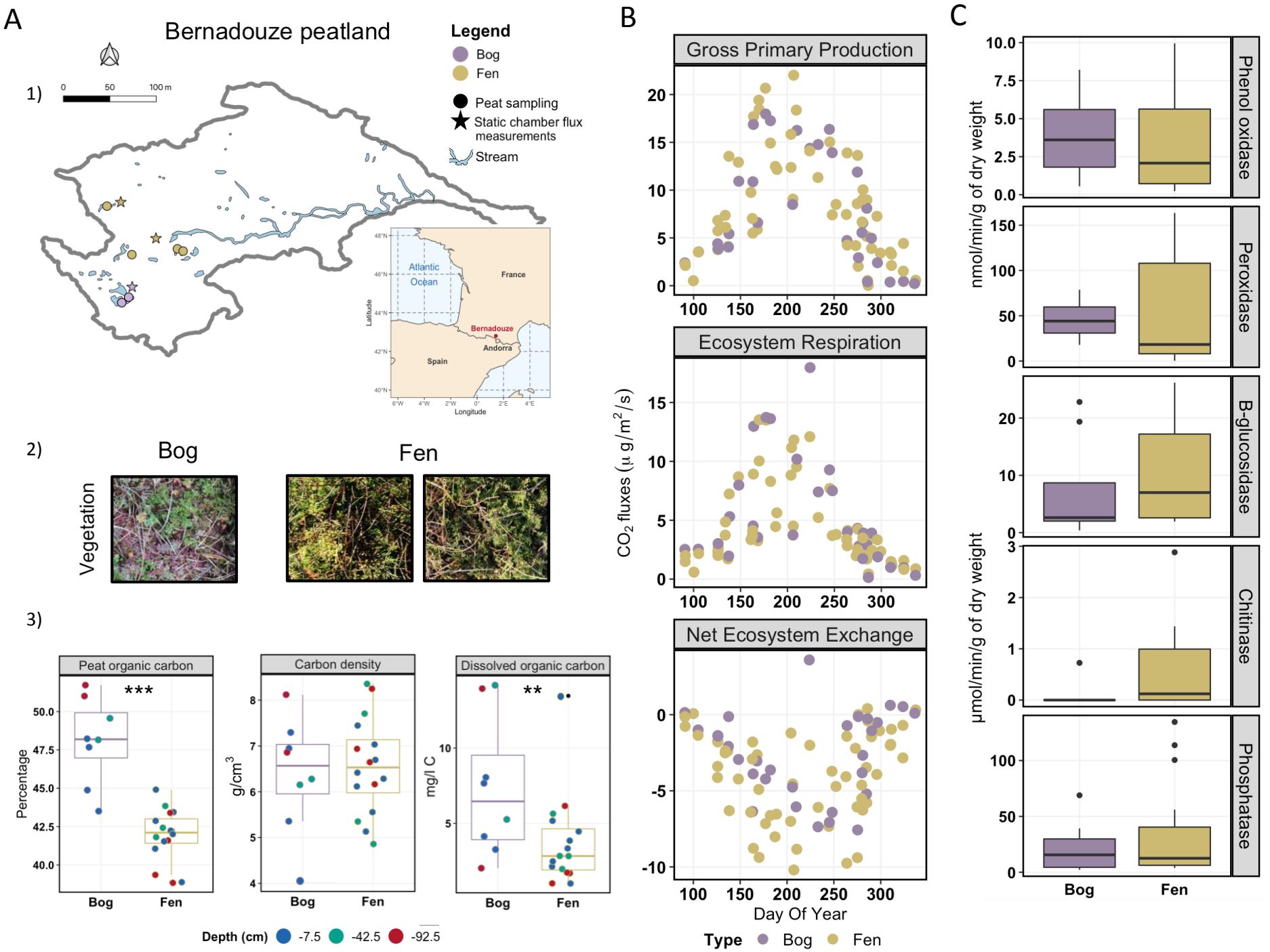

Figure 1. Location of the Bernadouze peatland and carbon dynamics (peat organic carbon, dissolved organic carbon, atmospheric carbon fluxes and microbial enzymatic activities related to OM degradation).

*A. 1) Location of the Bernadouze peatland and sampling sites. The dots represent the locations of peat samplings and the stars the location of static chamber flux measurements. Purple and yellow color code indicates the bog and fen sites respectively. 2) Representative vegetation covers of the bog and the fen. 3) Box plots of peat organic carbon and dissolved organic carbon concentration, with n=8 for bog and n=16 for fen. Stars indicate the level of significance (** if p-value < 0.01 and *** if p-value < 0.001).*

B. Atmospheric carbon fluxes over six-year period. Gross Primary Production (GPP), Ecosystem Respiration (ER) and Net Ecosystem Exchange (NEE), measured in the bog (30 measures across 6 years) and the fen (57 measures across 6 years) using a static chamber flux.

C. Comparison of enzymatic activities involved in the degradation of organic matter between bog (n=8) and fen (n=16).

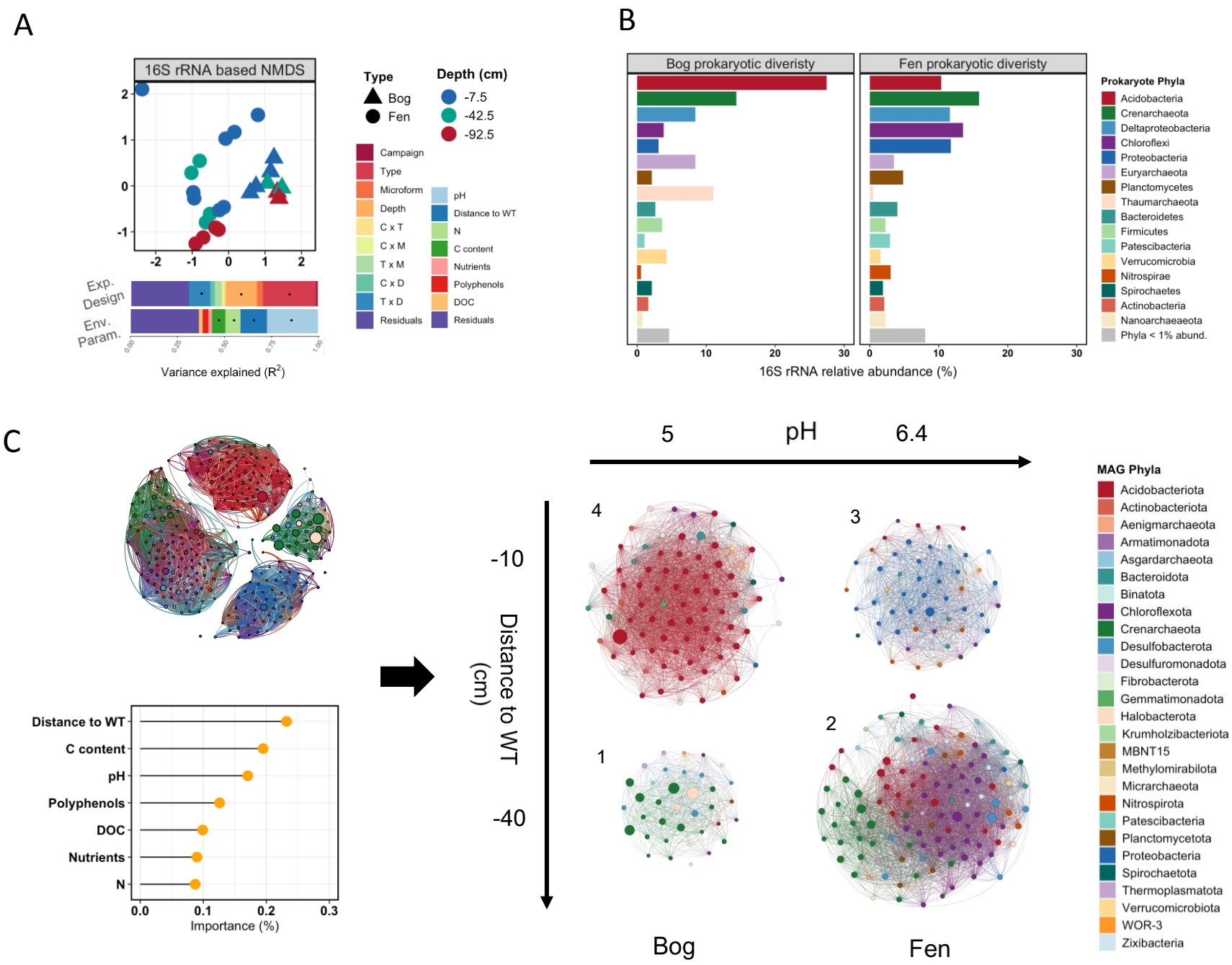

Figure 2. Environmental drivers of the microbial communities, prokaryotic diversity based on 16S rRNA gene and characterization of the Bernadouze metagenome-assembled genomes (290 dereplicated MAGs).

A. Non-metric multidimensional scaling (NMDS) plot of 16S rRNA gene data based on Bray-Curtis distance (stress: 0.10). Below the NMDS, analyses of variance testing the effect of experimental design (Exp. Design): campaign, peatland type, microform, depth, and all possible two-way interactions, and environmental variables (Env. Param.): pH, distance to WT, DOC, C content, N, polyphenols, nutrients, on microbial community structure (16S rRNA based data) using PerMANOVA. Black dots indicate significant correlations (if p-value < 0.05).

B. Relative abundance of prokaryotic phyla in the bog and the fen, estimated by unassembled 16S rRNA gene reads.

C. Abundance-weighted co-occurrence network based on Spearman correlations calculated from the recruitment values of the 290 unique MAGs with > 50% of completeness and < 5% of contamination (top left). Only significant edges are shown (coefficient > 0.6, p-value < 0.001). The size of the nodes is proportional to the cumulative abundance of MAGs in the 24 metagenomes. The importance of environmental variables predicting module configuration, estimated by a random forest classification model, is shown in the bottom left. Spatial location of MAGs was estimated using individual weighted means calculated for each environmental variable (pH and distance to WT) using RPKG data as abundance (right).

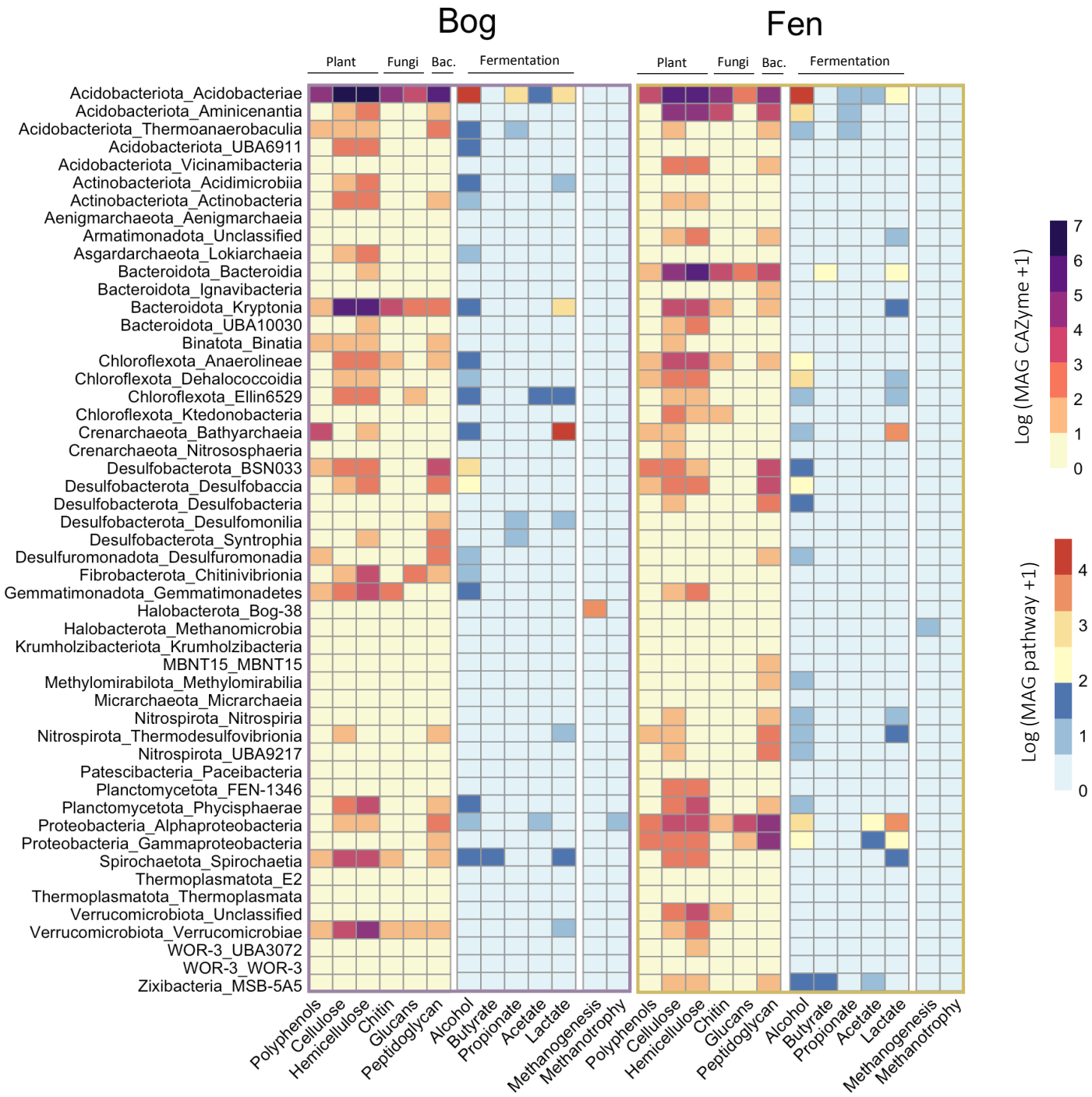

Figure 3. Predicted metabolic capacities of the Bernadouze MAGs.
Heatmap showing the abundance (log (abundance +1)) of MAGs-encoded CAZyme involved in plant biomass degradation (cellulose: GH1, GH3, GH116, GH5, GH6, GH9, GH12, GH45, GH8, AA9, AA10, GH7, GH48, hemicellulose: GH36, GH51, GH54, GH62, GH95, CE1, CE2, CE3, CE4, CE5, CE6, CE7, CE12, CE15, CE16, GH2, GH52, GH120, GH39, GH43, GH26, GH10, GH11, GH30, GH131, GH67, GH115, GH74, GH16, GH44, AA6), fungal biomass degradation (chitin: GH18, GH19, AA11, GH20 and glucans: GH17, GH64, GH81, GH128, GH55), bacterial biomass degradation (peptidoglycan: GH22, GH24, GH25, GH108, GH23, GH73, GH102, GH103, GH104) and polyphenol compounds degradation (K05909, AA1, AA2, K00422) in yellow to purple. The abundances of fermentative (alcohol: K00001, K00121, K04072, K13951, K13952, K13953, K13954, K13980, K18857, butyrate: K00634, K00929, K01896, propionate: K19697, K01026, acetate: K00625, K00925, K01905, K01067, lactate: K00016, K00101, K03778, K03777), methanogenic (K00399, K00401, K00402) and methanotrophic (K10944, K10945, K10946) pathways recovered in MAGs are in light blue to red. The metabolic capacities of MAGs in bog are shown in the left panels (purple frame) and in the right panels (yellow frame) for the fen. These capacities are summed at class-level and log transformed +1.

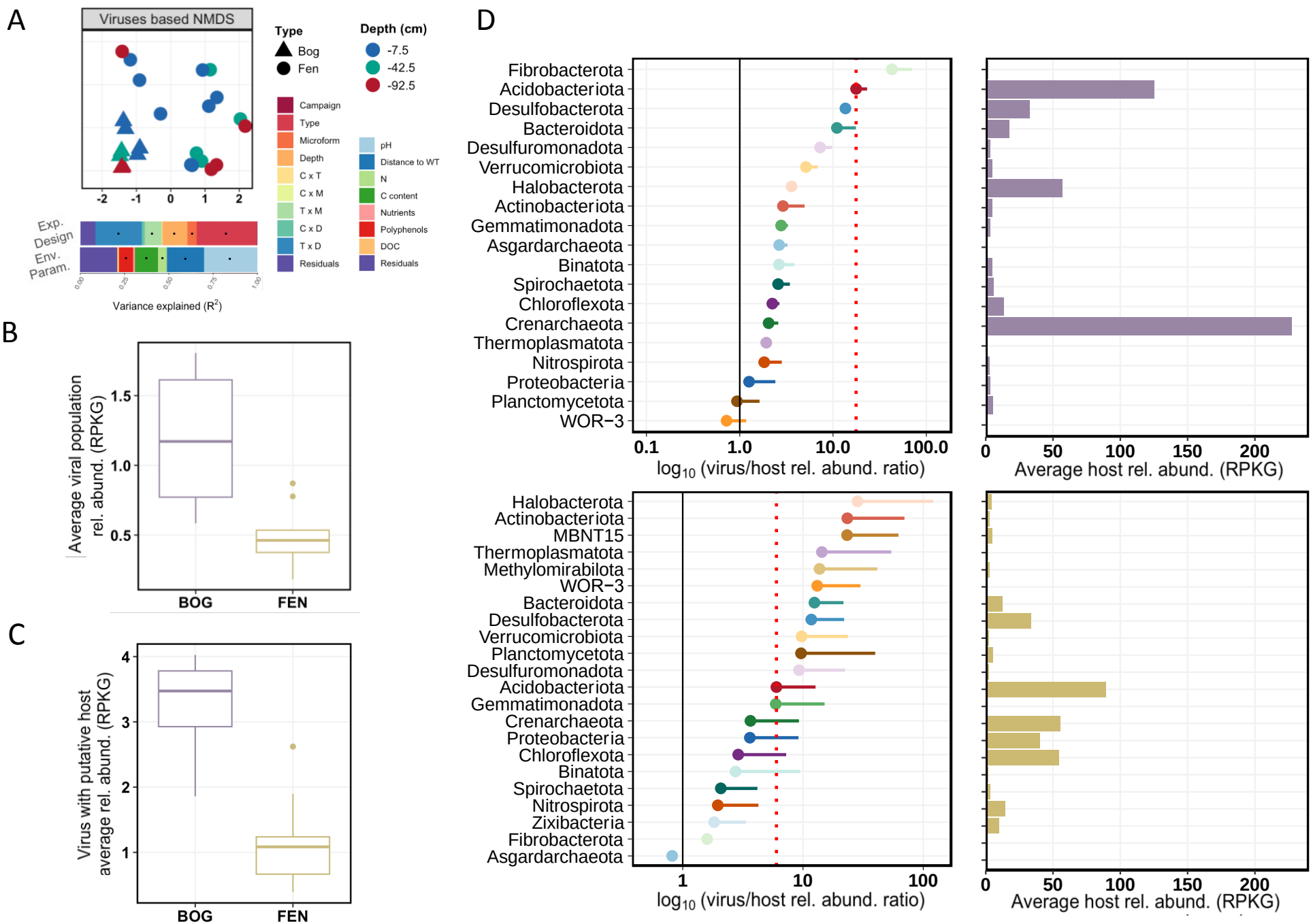

Figure 4. Environmental drivers and distribution of the viral populations at Bernadouze, predicted prokaryotic host and host-virus relationships in bog and fen

NMDS plot of the viral populations using Bray-Curtis distance (stress: 0.08). Below the NMDS, analyses of variance testing the effect of experimental design (Exp. Design): campaign, peatland type, microform, depth and all possible two-way interactions, and environmental variables (Env. Param.): pH, distance to WT, DOC, C content, N, polyphenols, nutrients, on viral composition using PerMANOVA. Black dots indicate significant correlation (if p-value < 0.05). Average viral population abundance in bog and fen samples (expressed in RPKG). Box plot representing the average abundance of the virus for which a putative host was identified (expressed in RPKG). Virus/host abundance ratios by host lineage. Abundances were calculated from read mapping to viral population and host genomes (both expressed in RPKG), respectively, in bog (top left panel) and in fen (bottom left panel). The dots indicate the mean ratio across samples (in bog n = 8, in fen n = 16), and the error bars indicate one standard deviation. The red line indicates the virus/host abundance ratio for the Acidobacteria phylum. The means host abundance in bog and fen are reported on the right panels.

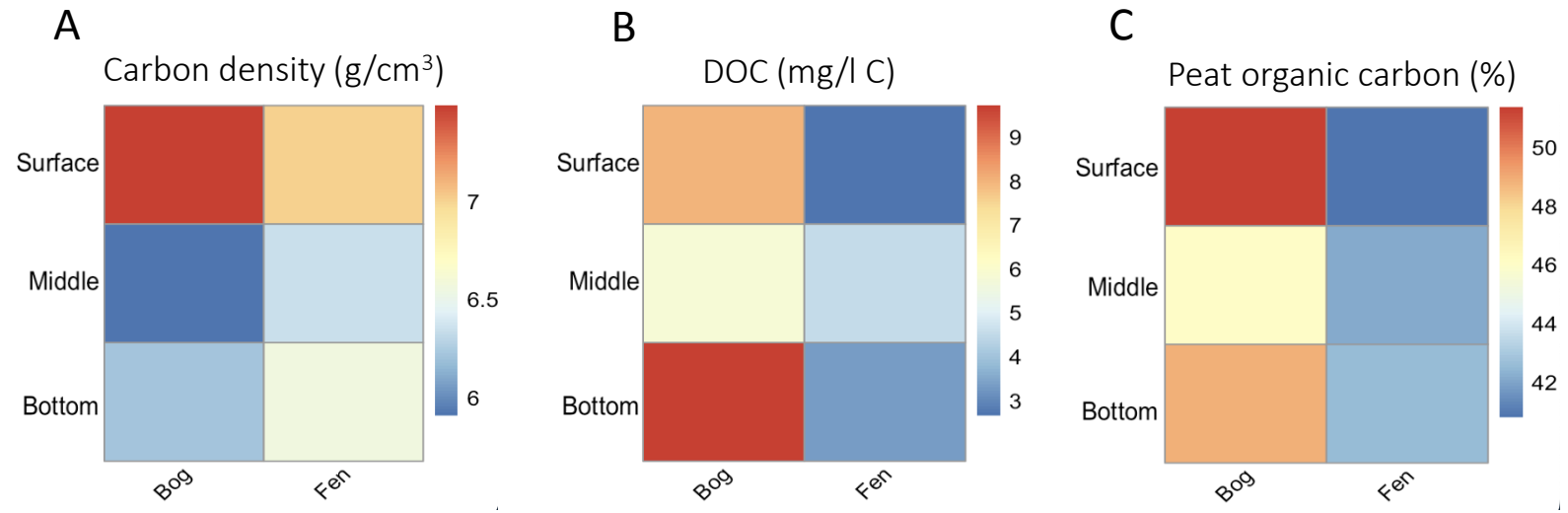

Figure S1. Carbon variations in bog and fens according to peat depth

Heatmap showing the variations of carbon density (A), dissolved organic carbon (B) and peat organic carbon (C) in bog (n=8) and fen (n=16).

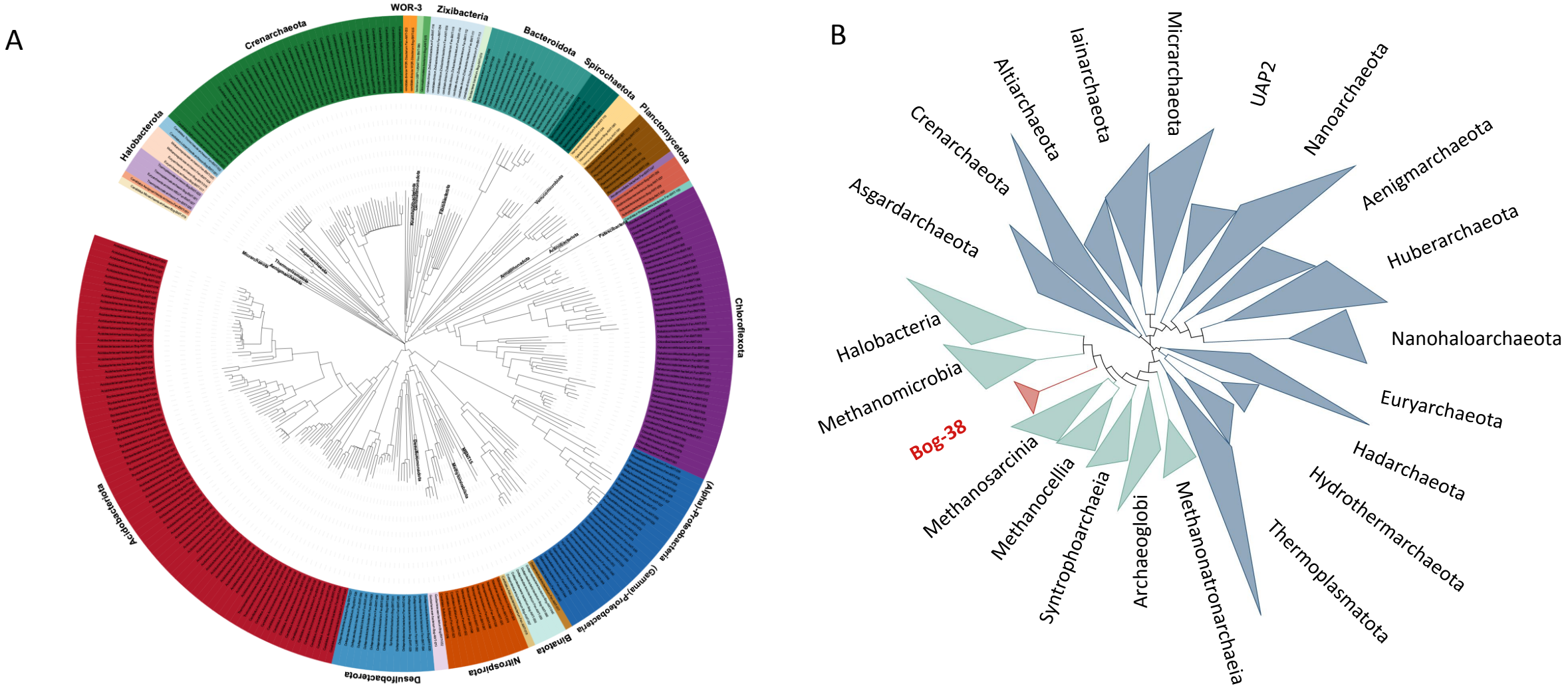

Figure S2. Maximum likelihood phylogenomic tree of the MAGs recovered from the Bernadouze peatland and position of the Bernadouze methanogen lineages within the archaeal phylogenetic tree

Maximum likelihood phylogenomic tree computed using GTDB-tk software, classifying each MAG according to its location in the reference tree, its relative evolutionary divergence and/or average nucleotide identity (ANI) with respect to the reference genomes. The tree was estimated based on the concatenated phylogeny of 120 bacterial single-copy marker genes or 122 archaeal single-copy marker genes. It includes 240 unique bacterial genomes and 50 unique archaeal genomes (> 50% of completeness and < 5% of contamination). Among them, Acidobacteriota (80 MAGs), Chloroflexota (44), Crenarchaeota (38), Proteobacteria (29), Bacteroidota (16) and Desulfobacterota (14) are the most represented phyla in the assemblage. In addition, 25 genomes belonging to phyla with a relative abundance of less than 1% according to 16S rRNA gene data were assembled, among which Aenigmarchaeota and Micrarchaeota (DPANN), Asgardarchaeota, Armatimonadota, Gemmatimonadota or Krumholzibacteriota.

Phylogenetic tree of archaea calculated using GTDB-tk software. Reference taxa were also plotted to identify the position of Bernadouze's methanogen lineages. To highlight the position of Bog-38 (in red), the branches are collapsed either at the phylum-level (in blue) or the class-level (in green). Four MAGs exhibiting capacity for hydrogenotrophic methanogenesis were recovered, two belonging to the Bog-38 class and two to Methanomicrobia. The present tree revealed that Bog-38 is a sister taxon of the clade Methanomicrobia/Halobacteria. All these taxa share a common ancestor with the clade Methanosarcina/Methanocellia.

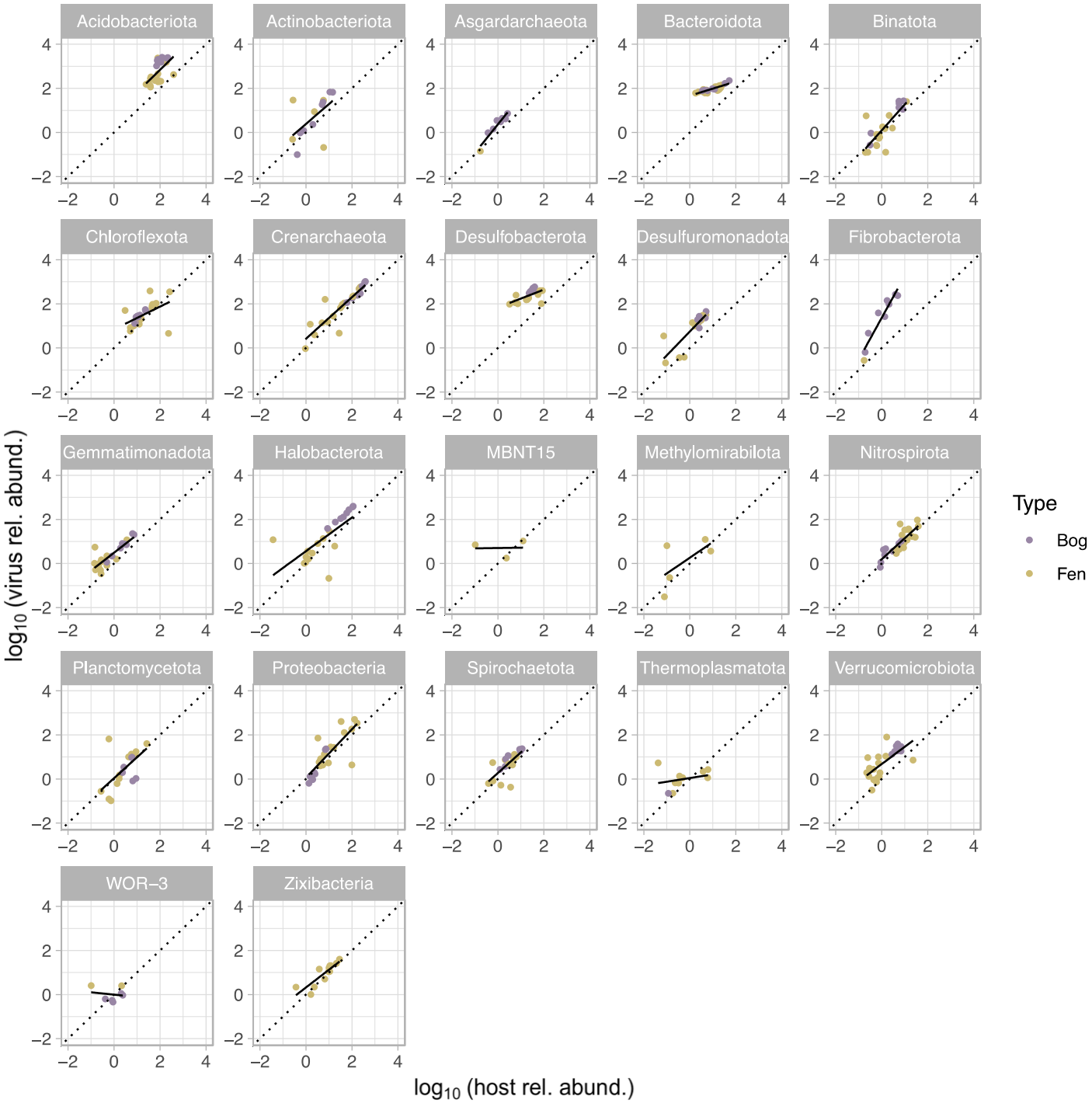

Figure S3. Host virus relationships in bog and fen

Positive relationships between virus abundance and host abundance at phylum level in the bog (n=8) and in the fen (n=16). Virus and host abundance were log-10 transformed. The dotted black line represents the 1:1 ratio, and the solid black line is the result of the linear regression. The bog samples are plotted in purple and the fen samples in yellow.